

1 **Consumption of atmospheric methane by the Qinghai–Tibetan**
2 **Plateau alpine steppe ecosystem**

3 **Hanbo Yun^{1,2,3}, Qingbai Wu^{1*}, Qianlai Zhuang^{3*}, Anping Chen^{4*} Tong Yu³, Zhou**
4 **Lyu³, Yuzhong Yang¹, Huijun Jin¹, Guojun Liu¹, Yang Qu³, Licheng Liu³**

5
6 **1. State Key Laboratory of Frozen Soil Engineering, Northwest Institute of Eco–**
7 **Environment and Resources, Chinese Academy of Sciences, Lanzhou, Gansu 730000,**
8 **China**

9 **2. Key Laboratory for Land Surface Process and Climate Change in Cold and Arid**
10 **Regions, Chinese Academy of Sciences, Lanzhou, 730000, China**

11 **3. Department of Earth, Atmospheric, and Planetary Sciences, Purdue University, West**
12 **Lafayette, Indiana 47907, USA**

13 **4. Department of Forestry and Natural Resources, Purdue University, West Lafayette,**
14 **Indiana 47907, USA**

15
16 ***Authors for correspondence: qbwu@lzb.ac.cn [Q. W.], qzhuang@purdue.edu [Q.Z.],**

17 **apchen1111@gmail.com [A.C.]**

18

19

20

A manuscript for *The Cryosphere*

21

22

May 30, 2018

23 **Abstract**

24 The Methane (CH₄) cycle on the Qinghai–Tibetan Plateau (QTP), the world’s largest high–
25 elevation permafrost region, is sensitive to climate change and subsequent freezing and thawing
26 dynamics. Yet, its magnitudes, patterns, and environmental controls are still poorly understood.
27 Here, we report results from five continuous year–round CH₄ observations from a typical alpine
28 steppe ecosystem in the QTP permafrost region. Our results suggest that the QTP permafrost
29 region was a CH₄ sink of -0.86 ± 0.23 g CH₄–C m⁻² yr⁻¹ over 2012 – 2016, a rate higher than that
30 of many other permafrost areas, such as the Arctic tundra in northern Greenland, Alaska, and
31 western Siberia. Soil temperature and soil water content were dominant factors controlling CH₄
32 fluxes, however, their correlations changed with soil depths, due to freezing and thawing
33 dynamics. This region was a net CH₄ sink in autumn, but a net source in spring, despite both
34 seasons experiencing similar top soil thawing and freezing dynamics. The opposite CH₄
35 source/sink function in spring versus in autumn was likely caused by the respective seasons
36 specialized freezing and thawing processes, which modified the vertical distribution of soil
37 layers that are highly mixed in autumn, but not in spring. Furthermore, the traditional definition
38 of four seasons failed to capture the pattern of the annual CH₄ cycle. We developed a new
39 seasonal division method based on soil temperature, bacterial activity, and permafrost active
40 layer thickness, which significantly improved the modelling of the annual CH₄ cycle.
41 Collectively, our findings highlight the critical role of fine–scale climate freezing and thawing
42 dynamics in driving permafrost CH₄ dynamics, which needs to be better monitored and modelled
43 in Earth system models.

44 **1. Introduction**

45 Since 2007, the global atmospheric methane concentration [CH₄] continues to rise, after
46 remaining stable between the 1990s and 2006 (Rigby et al., 2008; IPCC, 2013; Patra and Kort,
47 2016). Understanding mechanisms for this recent increase requires improved knowledge on CH₄
48 sources and sinks for regional and global CH₄ budgets (Kirschke et al., 2013; Zona et al., 2016).
49 However, estimates on global CH₄ emissions and consumptions are still highly uncertain (Spahni
50 et al., 2011; Kirschke, 2013). In particular, the bottom–up approach, which estimates CH₄
51 budgets using ground observations and inventory, overestimated the global CH₄ budget by 6~20
52 times, compared to the atmospherically constrained top–down approach (Zhu et al., 2004; Lau et
53 al., 2015). This discrepancy is partly due to limited monitoring data and to our poor
54 understanding of important factors regulating the production and consumption of CH₄ (Whalen
55 and Reeburgh, 1990; Dengel et al., 2013; Bohn et al., 2015).

56 The Qinghai–Tibetan Plateau (QTP) is the world’s largest high–elevation permafrost
57 region of 1.23×10^6 km² (Wang et al., 2000). The QTP is currently experiencing a rapid change
58 in climate, which affects freezing and thawing processes. The change in the freezing and thawing
59 dynamics profoundly impacts methanotrophy and methanogenesis, which consequently impacts
60 net CH₄ fluxes (Mastepanov *et al.*, 2013; Lau et al., 2015). However, due to the scarcity of year-
61 round monitoring data at high temporal resolution, we still know little about the size, seasonal
62 pattern, and underlying controls of climate and permafrost freezing and thawing, and the
63 resulting effects on CH₄ exchanges in the QTP permafrost region (Cao et al., 2008; Wei et al.,
64 2015a; Song et al., 2015;). This knowledge gap also hampers our capacity to predict and
65 understand QTP permafrost CH₄ cycles under current and projected future climates.

66 Here, we report results from a 5-year continuous *in situ* monitoring of CH₄ dynamics
67 with an eddy covariance (EC) technique at the Beilu'he Research Station, which is a
68 representative site for QTP permafrost heartland. The site was covered by alpine steppe
69 vegetation from January 1st, 2012 to December 31st, 2016. The primary aims of this investigation
70 are to understand (1) the long-term annual and seasonal variation of the methane budget for a
71 typical alpine permafrost site in the QTP, and (2) the environmental factors controlling these CH₄
72 variations and possible underlying mechanisms. In addition, while the consumption and
73 production of ecosystem methane are known through microbial activities, conventional
74 investigations on seasonal methane fluxes usually used climate or vegetation defined "seasons".
75 Therefore, a third research goal of this current study is to investigate if the classical vegetation
76 productivity-based definition of growing season will be useful for defining the methane flux
77 seasonality.

78 There are three advantages of our data acquisition system. First, the EC system recorded
79 the data of CH₄ fluxes, climate, and soil properties every half hour. As the QTP permafrost is
80 characterized by a rapidly changing climate and a rapidly changing soil freezing and thawing
81 dynamics, even over a time period as short as one day, different aerobic or anaerobic soil
82 environments that favor different types of CH₄ bacteria may change (Rivkina et al., 2004; Lau et
83 al., 2015). Thus, high-resolution *in situ* monitoring data enables us to quantify CH₄ exchange
84 patterns from diel to annual time-scales and investigate their major environmental drivers.
85 Second, our field investigation spanned five full calendar years, including both plant growing
86 and non-growing seasons. Observations of the plant non-growing season, which accounts for
87 two-thirds of a year, are very rare in current literature (Song et al., 2015). Third, the EC system
88 we used overcame some technical problems caused by the often used static chambers, including

89 limited representation of local site heterogeneity and additional heating of the soil surface
90 (Chang et al., 2014; Wei et al., 2015b).

91 **2. Methods**

92 **2.1 Site Description**

93 The research site, Beilu'he permafrost research station (34° 09' 006" N, 92° 02' 080" E),
94 is located in the alpine steppe continuous permafrost area of the northern QTP, about 320
95 kilometers southwest of Golmud, Qinghai Province (Figure 1). At an elevation of 4765 meters,
96 the air is thin with only 0.6 standard atmospheric pressure. According to *in situ* observations, the
97 site receives solar radiation of about 213.10 W m⁻². The non-growing season is long and cold,
98 with 225 days per year having an annual air temperature of -18 °C on average from 2012 to
99 2016. The site's growing season is short and cool, with 140 days per year from 2012 to 2016,
100 and a mean annual air temperature of 4.6 °C. According to the site drilling exploration, the
101 permafrost depth can extend to 50 – 70 m below ground, and the thickness of the active layer
102 (ALT) is about 2.2 – 4.8 m (Wu et al., 2010a). The soil is composed of Quaternary fine sand or
103 silt (Table 1), overlying on Triassic mudstone or weathered marl. Dominant plant species
104 include: *Carex moorcroftii* Falc. ex Boott, *Kobresia tibetica* Maxim, *Androsace*
105 *tanggulashanensis*, and *Rhodiola tibetica*. Vegetation coverage is approximately 33.5% and the
106 average plant height is 15 cm.

107 **2.2 Eddy Covariance observations**

108 We have continuously monitored CH₄, carbon dioxide (CO₂), water (H₂O), and heat flux
109 using a standard eddy covariance system tower 3 meters above the ground. CH₄ flux was measured
110 with an open-path CH₄ analyzer system (Figure 1d; LI-7700, LI-COR Inc., Lincoln, NE, USA).

111 The precision is 5 ppb, with RMS noise at 10 Hz and 2000 ppb. The instrument was placed on site
112 on August 8th, 2011, and then connected to a three-dimensional sonic anemometer (heat and water
113 flux; CSAT3, Campbell Scientific, and Logan, UT, USA; the precision is 0.1 °C with an accuracy
114 within 1% of reading for half-hour measurements) and an open-path infrared gas analyzer (CO₂
115 flux; LI-7500A, LI-COR Inc., Lincoln, NE, USA; the precision is 0.01 μmol m⁻² s⁻¹ with an
116 accuracy within 1% of reading for half-hour measurements, zero drift per °C is typically ± 0.1
117 ppm) on January 1st, 2012, when the system worked steadily. Monitoring data was recorded and
118 stored at 10 Hz using a data logger (LI-7550, LI-COR Inc., Lincoln, NE, USA).

119 The operation, calibrations, and maintenance of the EC system followed standard
120 procedures. To reduce the LI-7500A surface heating/cooling influence on CO₂ and H₂O molar
121 densities in tough environments, each year “summer style” was used in Li-7500A, in which
122 surface temperature setting is 5 °C during May 1st to September 30th. “Winter style” was used from
123 October 1st to the next year April 30th in Li-7500A, in which surface temperature setting is -5 °C.
124 Calibrations of CO₂, water vapor, and dew point generator measurements for LI-7500A analyzers
125 were performed regularly by the China Land-Atmosphere Coordinated Observation System
126 (CLAROS). Up-and-down mirrors of LI-COR 7700 were cleaned regularly every 30 days to
127 make sure the signal strength was stronger than 80. All of these instruments were powered by
128 solar-panel and battery.

129 **2.3 Micrometeorological and Soil Measurements**

130 A wide range of meteorological variables were measured by a standard automatic
131 meteorological tower 3 meters above the ground and 5 meters north of the eddy covariance
132 tower. Net radiation (R_n) and albedo were measured with a four-component radiometer (R_n;
133 CNR-1, Kipp and Zonen, the Netherlands). Air temperature (T_{air}), air relative humidity, and

134 atmospheric pressure were measured with a temperature and humidity sensor (HMP45C, Vaisala
135 Inc., Helsinki, Finland) in the meteorological tower. A rain gauge (TE525MM, Texas Electronics
136 Inc., Dallas, TX, USA) was used to measure precipitation. Wind speed and direction were
137 observed using a propeller anemometer placed on the top of the meteorological tower.

138 We also measured soil heat fluxes, soil temperature and soil relative water content (SWC).
139 In August 2010, we installed sensors for soil environment and surface energy exchange
140 monitoring 10 m apart from the eddy covariance tower. Two self-calibrating soil heat flux (SHF)
141 sensors (HFP01) were placed 5 cm and 15 cm below the ground. A group pF-Meter sensor
142 (GEO-Precision, Germany) was embedded in the soil under the meteorological tower to measure
143 soil temperature (T_{soil}) at 0 cm, 5 cm, 10 cm, 15 cm, 20 cm, 30 cm, 40 cm, 50 cm, 70 cm, 80 cm,
144 100 cm, 150 cm, 160 cm, and 200 cm depth. The pF meter sensors also measured SWC at 10 cm,
145 20 cm, 40 cm, 80 cm, and 160cm depth.

146 All of above environmental parameters were synchronously monitored with eddy
147 covariance, and the data was recorded every 30 minutes by CR3000 (Data logger, Campbell Data
148 Taker Ltd, Salt Lake City, UT, USA). The air temperature sensors, the humidity sensors, and the
149 pF meter sensors were calibrated in the State Key Laboratory of Frozen Soil Engineering at the
150 Chinese Academy of Sciences in order to ensure the measurement accuracy was within ± 0.05 °C
151 and $\pm 5\%$, respectively.

152 We also sampled soil profiles for soil physical and chemical measurements with one 1 m \times
153 1 m \times 2 m pit 10 m apart from the eddy covariance tower in August 2010. Five profile samples
154 were taken from the pit at depths 0 – 20 cm, 20 – 50 cm, 50 – 120 cm, 120 – 160 cm, and
155 160 – 200 cm. Sampling at each depth was repeated five times and the samples of the same

156 depths were then well mixed. After that, the mixed soil sample of each depth was stored in
157 aluminum boxes and carefully sealed to prevent gas exchanges with air. The clod method was
158 used to investigate the field wet bulk density (weight of soil per unit volume; Cate and Nelson,
159 1971). The soil moisture content was calculated gravimetrically by the ratio of the mass of water
160 present to the oven-dry (60 °C for 24 hour) weight of the soil sample. The soil organic carbon
161 (SOC) content of the air-dried soil samples was analyzed using the wet combustion method,
162 Walkley-Black modified acid dichromate digestion, FeSO₄ titration, and an automatic titrator.
163 Total nitrogen (TN) and pH were measured using standard soil test procedures from the Chinese
164 Ecosystem Research Network.

165 To understand the potential effect of soil thawing and freezing dynamics on CH₄ fluxes,
166 we also reconstructed and verified semi-monthly data of soil active layer thickness (ALT).
167 Following Muller's original definition, ALT is the maximum thaw depth in the late autumn using
168 a linear interpolation of T_{soil} profiles between two neighboring points above and below the 0 °C
169 isotherm (Muller, 1947). We used records of the soil thawing thickness measured with a self-
170 made geological probe to verify the ALT data semi-monthly. More information about the
171 measurement procedure was previously described by Wu and Zhang (2010a).

172 **2.4 Microbial Activity**

173 To understand how soil microbial activity may have impacted the CH₄ fluxes, we sampled
174 100 g soils for soil microbial activity measurements. These soils were obtained using a soil
175 sample drill device (Ø=0.03 m), with depths of 0 – 25 cm taken every 5 days within 100 m of the
176 eddy covariance tower. The sampled soil was fully mixed and divided into two equal parts. Each
177 part was then stored in sterilized aluminum boxes and then placed in liquid nitrogen, before
178 sending to the lab for microbe RNA extraction. We then used a real-time PCR method to

179 genetically test methanotrophic / archaeal methanogens, and the procedure was repeated three
180 times for each sample. By setting the maximum methanotrophic / archaeal methanogens gene
181 expression cyclic number as 1, we calculated the variety coefficient of methanotrophic and
182 archaeal methanogens gene expressions (ΔI and ΔII , respectively; %) with equation (1):

$$183 \quad \Delta_i = \frac{x_i}{X_{Max}} \quad \dots \quad (1)$$

184 Δ_i is for the i^{th} methanotrophic/archaeal methanogens gene expression; x_i is the
185 methanotrophic / archaeal methanogen gene expression cyclic number of the i^{th} time; X_{Max} is the
186 maximum methanotrophic / archaeal methanogen gene expression cyclic number of the soil
187 group from 2012 to 2016.

188 **2.5 EC Data Processing and Data Filtering**

189 Data collected from January 1st, 2012 to December 31st, 2016 was used in this study. Before
190 processing, we removed data that was recorded at the time of precipitation events or with LI-7700
191 signal strength under 85. We first processed the raw data in EddyPro (version 6.2.0, LI-COR,
192 Lincoln, NE, USA). We adopted standardized procedures recommended in Lee et al. (2006) to
193 process half-hourly flux raw measurements to ensure their quality.

194 1) Data was processed through statistical analysis in EddyPro including: spike removal
195 (accepted spikes < 5% and replaced spikes with linear interpolation), amplitude resolution (range
196 of variation: 7.0σ , number of bins: 100, accepted empty bins: 70%), drop-outs (percentile defining
197 extreme bins: 10, accepted central drop-outs: 10%, accepted extreme drop-outs: 6%), absolute
198 limits ($-30 \text{ m s}^{-1} < U < 30 \text{ m s}^{-1}$, $-5 \text{ m s}^{-1} < W < 5 \text{ m s}^{-1}$, $-40 \text{ }^\circ\text{C} < T_s < 40 \text{ }^\circ\text{C}$, $200 \text{ } \mu\text{mol mol}^{-1} < \text{CO}_2$

199 < 500 $\mu\text{mol mol}^{-1}$, 0 $\mu\text{mol mol}^{-1}$ < H_2O < 40 $\mu\text{mol mol}^{-1}$, 0.17 μmol < CH_4 < 1000 μmol), Skewness
200 and kurtosis (-2.0 < Skewness lower limit < -1.0, 1.0 < Skewness up limit < 2.0; 1.0 < Kurtosis
201 lower limit < 2.0, 5.0 < Kurtosis upper limit < 8.0), discontinuities (hard-flag threshold: $U = 4.0$,
202 $W = 2.0$, $T_S = 4.0$, $\text{CO}_2 = 40$, $\text{CH}_4 = 40$, and $\text{H}_2\text{O} = 3.26$; soft-flag threshold: $U = 2.7$, $W = 1.3$, T_S
203 $= 2.7$, $\text{CO}_2 = 27$, $\text{CH}_4 = 30$, and $\text{H}_2\text{O} = 2.2$), angle of attack (minimum angle of attack = -30,
204 maximum angle attack = 30, accepted amount of outliers = 10%), and steadiness of horizontal
205 wind (accepted wind relative instationarity = 0.5) (Vickers and Mahrt, 1997; Mauder et al., 2013).

206 2) The data was then corrected using atmosphere physical calculations expressed by: axis
207 rotations of tilt correction (double rotation), time lags compensation (covariance maximization),
208 and compensating density fluctuations of Webb–Pearman–Leuning (Webb et al., 1980). When
209 CO_2 and H_2O molar densities are measured with the LI-COR 7500 / LI-COR 7500A in cold
210 environments (low temperatures below -10 °C), a correction should be applied to account for the
211 additional instrument-related sensible heat flux, due to instrument surface heating / cooling. Thus,
212 we implemented the correction according to Burba et al. (2008), which involves calculating a
213 corrected sensible heat flux (H') by adding estimated sensible heat fluxes from key instrument
214 surface elements, including the bottom window (H_{bot}), top window (H_{top}), and spar (H_{spar}) to the
215 ambient sensible heat flux (H):

$$216 \quad H' = H + H_{bot} + H_{top} + 0.15 \times H_{spar} \quad (2)$$

217 3) Quality assurance (QA) / quality control (QC) were ensured through spectral analysis
218 and corrections analysis in EddyPro. Spectra and co-spectra calculations used power-of-two
219 samples to speed up the Fast Fourier Transform (FFT) algorithm. Here we checked the “Filter
220 (co)spectra according to Vickers and Mahrt (1997) test results” box in EddyPro, which would then

221 disregard EC flux time series that would likely create artifacts in spectral and co-spectral shapes.
222 We also used the Mauder and Foken (2004) micrometeorological quality tests embedded in
223 EddyPro to filter low quality EC time series data. Low-frequency range spectral correction was
224 done considering high-pass filtering effects. High-frequency range spectral correction was done
225 considering low-pass filtering effects (Moncrieff et al., 2004).

226 4) We chose values of “0”, “1”, “2” to flag the processed flux data into three quality classes
227 in EddyPro. The combined flag attains the value “0” for best quality fluxes, “1” for fluxes suitable
228 for general analysis, such as annual budgets, and “2” for fluxes that should be discarded from the
229 results dataset. For our dataset, approximately 67% of the data fell into Class 0, 12% in Class 1,
230 and 21% in Class 2.

231 5) Our analysis indicated that, under average meteorological conditions, 80% of the flux
232 (footprint) came from an area within 175 m of the eddy covariance tower.

233 In addition, we also adopted the method in Burba et al. (2008) to adjust the half-hour flux
234 data, to avoid apparent measurement errors. In doing this, we rejected half-hour flux data that fell
235 into one of the following situations: (1) incomplete half-hour measurements, (2) measurements
236 under rain impacts, (3) nighttime measurements under stable atmospheric conditions (friction
237 velocity $U^* < 0.1 \text{ m s}^{-1}$), and (4) abnormal values detected by a three-dimensional ultrasonic
238 anemometer. This screening resulted in the rejection of about 20.7% of all the flux data.

239 After the above data quality control, there was a 28.7% data gap for CH₄ fluxes over the
240 entire period. These data gaps were then filled according to the method described in literature
241 (Falge et al., 2001; Papale et al., 2003). We used a linear interpolation to fill the gaps if they were
242 less than 2 hours, a method described in Falge *et al.* (2001) to fill gaps greater than 2 hours, but

243 less than 1 day, and an artificial neural network approach as described in Papale et al. (2003) and
244 Dengel et al. (2013) to fill gaps greater than 1 day.

245 The quality of the dataset was evaluated using the equation of energy closure:

$$246 \quad EBR = \sum (H + \lambda E) / \sum (R_n - G - S) \quad (3)$$

247 where the *EBR* is surface energy balance ratio, *H* is heat flux, λE is latent heat, *R_n* is net
248 radiation, *G* is soil heat flux (SHF), and *S* is heat storage of the vegetation canopy. As vegetation
249 coverage at this research site is sparse, *S* is ignored. From 2012 to 2016, the average *EBR* value at
250 the Beilu'he EC site was about 0.675, falling within the range of 0.34 to 1.69 in an analysis of
251 energy balance closure for global FLUXNET sites (Wilson et al., 2002).

252 We analyzed two different major sources of CH₄ flux gap-filling uncertainty. The first kind
253 of uncertainty came from U* threshold estimate. Following Burba et al. (2008), we excluded the
254 probably false low CH₄ flux at low U*. However, it was difficult to determine the value for the
255 U* threshold. For instance, when choosing a lower U* threshold, the associated lower flux would
256 contribute to the gap filling and the annual gross (Loescher, et al., 2006). Here we used the variance
257 from 5% to 95% of the bootstrapped values to provide an estimate on the uncertainties caused by
258 different U* thresholds. The second uncertainty source was due to insufficient power supply. In
259 this research, all instrument power was supplied by solar panels. Extended periods of rainy, cloudy,
260 and snowy weather would cause the instrument to stop working due to an insufficient power supply.
261 When we used the gap-filling method mentioned above, it would cause the CH₄ flux to deviate
262 from the true value. To our knowledge, the CH₄ flux data was largely uncertain under rainy
263 conditions.

264 **2.6 New classification system of the four seasons based on microbial activities classification**

265 We redefined the four seasons of spring, summer, autumn, and winter based on the
266 microbial activity parameters of the new seasons (Figure 2), ALT variability coefficients (ALT
267 variability coefficient = $(ALT_{i+1} - ALT_i) / ALT_{Max}$, where ALT_{Max} is the maximum of ALT per
268 year), and T_{soil} . Below, we describe the start date of each season (the end date of a season is the
269 day immediately before the start of the next season).

270 Spring starts at the first day of two consecutive observation periods fulfilling both (1) $(\Delta II +$
271 $\Delta I) / 2 \geq 15\%$, and (2) the ALT variability coefficient ≥ 0.05 .

272 Summer starts on the first day of two consecutive observation periods when (1) $(\Delta II + \Delta I) /$
273 $2 \geq 45\%$, (2) ALT variability coefficient ≥ 0.35 , and (3) five successive days with T_{soil} at 40
274 cm soil depth $\geq 0^\circ\text{C}$.

275 Autumn starts on the first day of two consecutive observation periods when (1) $(\Delta II + \Delta I) /$
276 $2 \geq 55\%$, (2) the ALT variability coefficient ≥ 0.60 , and (3) five successive days the T_{soil} of 10
277 cm $< 5^\circ\text{C}$.

278 Winter starts on the first day of two consecutive observation periods that (1) $(\Delta II + \Delta I) / 2$
279 $< 15\%$ and the ALT variability coefficient < 0.05 .

280 To test the robustness of our new seasonal division method in our methane cycle analysis,
281 we compared empirical CH_4 flux estimates using different season definitions (Table 2). In
282 addition to our new method that was based on top soil microbe activity, T_{soil} of 0 – 40 cm, and
283 permafrost active layer variability (hereafter refer to as SMT), we also used three conventional
284 methods, based on (i) vegetation cover and temperature change (VCT), (ii) based on Julian

285 months (JMC), and (iii) based on vegetation phenology change (VPC). The VCT method splits a
286 year into a plant growing season and a non-growing season; the JMC method assumes May to
287 October as a plant growing season, and November to the following April as a non-growing
288 season; and the VPC method defines a plant growing season as the period between the time when
289 all dominant grass species (*Carex moorcroftii* Falc. ex Boott, *Kobresia tibetica* Maxim,
290 *Androsace tanggulashanensis*, *Rhodiola tibetica*) germinate and that when they all senesce.

291 **2.7 Statistical Analyses**

292 To understand the connections between CH₄ fluxes and associated environmental factors,
293 we performed a series of statistical analyses, including correlation, principal component analyses
294 (PCA), and linear regression analyses, in IBM SPSS (IBM SPSS Statistics 24; IBM, Armonk
295 NY, USA). Specifically, we used bivariate correlation to examine pairwise relationships between
296 environmental factors and CH₄ fluxes. We also used PCA and linear regressions to explore the
297 sensitivity of CH₄ fluxes to simultaneous environmental fluctuations in wind speed, T_{air}, air
298 relative humidity, Rn, vapor pressure deficit (VPD), albedo, SHF, SWC, and T_{soil}. Before
299 performing PCA and linear regressions, the entire dataset was examined for outliers (Cook's
300 Distance, < 0.002), homogeneity of variance (Levene test, $p < 0.05$), normality (Kolmogorov–
301 Smirnov test, smooth line for histogram of Studentized residuals), collinearity (variance inflation
302 factor, $0 < VIF < 10$), potential interactions (t -test, $p < 0.05$), and independence of observations
303 (t -test, $p < 0.05$).

304 We performed structural equation modeling (SEM) to evaluate the effects of
305 environmental variables on CH₄ fluxes for different seasons. SEM is a widely-used multivariate
306 statistical tool that incorporates factor analysis, path analysis, and maximum likelihood analysis.
307 This method uses *priori* knowledge of the relationships between focus variables to verify the

308 validity of hypotheses. Here we performed SEM analyses with AMOS 21.0 (Amos Development
309 Corporation, Chicago, IL, USA). All data are presented as mean values with standard
310 deviations.

311 **3. Results**

312 **3.1 Meteorological Conditions**

313 We first reported the statistics of the meteorological conditions at the Beilu'he Permafrost
314 Weather Station between 2012 to 2016. Mean annual T_{air} was $-4.5\text{ }^{\circ}\text{C}$ (Supplementary Figure 1),
315 with minimum and maximum mean diel temperatures of $-21.6\text{ }^{\circ}\text{C}$ (12th January, 2012) and $13.8\text{ }^{\circ}\text{C}$
316 (28th July, 2015), respectively. Average net radiation was 82.8 Wm^{-2} , with the maximum in August
317 (136.2 Wm^{-2} ; Supplementary Figure 2). The average VPD was about 0.3, with maximum and
318 minimum values of 0.98, and 0.02, respectively (Supplementary Figure 3). Mean annual
319 precipitation was 335.4 mm (Figure 3), which was primarily based on rain and snowfall (only
320 occupied 7%). Maximum and minimum precipitation was encountered in 2013 (488.3 mm), and
321 2015 (310.0 mm), respectively. The majority of precipitation, approximately 92%, occurred
322 hereby in the summer. During the winter, precipitation was rare with mean values around 6.7 mm.
323 Spring was another important rainfall period besides summer, with mean precipitation being about
324 37.5 mm, or 8~17% of the total.

325 The Beilu'he site is windy during most of the year (Supplementary Figure 4). Its annual
326 average speed was 4.4 m s^{-1} from 2012 to 2016, while the principal direction of the strongest winds
327 were from the southwest. Late autumn, winter, and early spring drought brought increased risks of
328 dust blowing days, with an average of 122 days within a year. Its summer average wind speed was
329 about 3.30 m s^{-1} , predominantly driven by the southwest wind.

330 The SWC and T_{soil} variability from 2012 to 2016 at the field site are summarized in
331 Supplementary Figures 5 and 6, respectively. Mean SWC of depths 10 cm, 20 cm, 40 cm, 80 cm,
332 and 160 cm were 14%, 9%, 8%, 14%, and 19%, respectively. T_{soil} of depths <100 cm corresponded
333 with the T_{air} changes, but showed stronger differences at depths >100 cm. The T_{soil} at 200 cm depth
334 showed a remarkable difference from that of other layers. The reason could be the occurrence of
335 peat in this layer, and that, during winter, the peat layer was not completely frozen. Supplementary
336 Figure 7 shows SHF half-hour and diel scale variability of 5 cm and 15 cm depth. The annual mean
337 value of SHF at 5 cm and 15 cm depth is 7.6 W m^{-2} and 6.8 W m^{-2} , respectively.

338 Finally, Supplementary Figure 8 shows the site's average soil freezing and thawing
339 dynamics observed from January 2012 to December 2016. The average ALT is 4.4 m from 2012
340 to 2016. At 40 cm depth the duration of the active layer ranged from 174 to 188 days, with an
341 average variation of up to 14 days.

342 **3.2 Annual, Seasonal and Diel Variabilities of Methane Fluxes**

343 Our results indicated that the Beilu'he site was a CH_4 sink, with an annual mean strength
344 of $-0.86 \pm 0.23 \text{ g CH}_4\text{-C m}^{-2}$ (95% confidence interval; negative values mean CH_4 sinks, positive
345 values mean CH_4 sources). The strength of the CH_4 sink varies across different years from -0.57
346 $\pm 0.27 \text{ g CH}_4\text{-C m}^{-2} \text{ yr}^{-1}$ in 2015, to $-1.49 \pm 0.38 \text{ g CH}_4\text{-C m}^{-2} \text{ yr}^{-1}$ in 2014 (Figure 3). The amount
347 of gene expression by methanogens and methanotrophs at 0 – 25 cm soils in March and
348 November, for instance, were about 16.8% and 35.6%, respectively, suggesting strong microbial
349 activities even during the cold and dry plant non-growing season (Figure 2).

350 We also clearly observed CH_4 seasonal variations (Supplementary Figure 9) in both the
351 amount of CH_4 exchanges and their diel cycles (Figure 4). Across different seasons the footprint

352 of the monitored CH₄ flux changed following the change of the prevalent wind direction. In
353 winter and spring, the major footprint was from east of the EC tower; while in summer and
354 autumn, the major footprint was from the EC tower's west and north (Supplementary Figure 4).

355 In winter, the net CH₄ flux at the Beilu'he site was an atmospheric source, with an
356 average annual rate of $0.41 \pm 0.16 \text{ g CH}_4\text{-C m}^{-2} \text{ yr}^{-1}$ or $4.35 \pm 0.33 \text{ mg CH}_4\text{-C m}^{-2} \text{ d}^{-1}$
357 (Supplementary Figure 9a). It should also be noted that since the investigation started January 1st,
358 2012, and ended on December 31st, 2016, the 2011 ~ 2012 and 2016 ~ 2017 winters were only
359 about half of the regular length. The diel CH₄ cycle of an average winter day was characterized
360 by one single emission peak around 10:30am ~ 17:30 pm (Figure 4a1-4f1).

361 In spring, the Beilu'he site was a CH₄ source of $0.90 \pm 0.37 \text{ g CH}_4\text{-C m}^{-2} \text{ yr}^{-1}$
362 (Supplementary Figure 9b), accounting for 53% of annual CH₄ emissions, or $1.81 \pm 0.22 \text{ mg}$
363 $\text{CH}_4\text{-C m}^{-2} \text{ d}^{-1}$. For a typical spring day (Figure 4a2-4e2), diel CH₄ emission usually started at
364 around 10:00 am ~ 10:30 am, when the thin ice layer on the soil surface started to thaw. It then
365 reached the peak at 12:30 pm ~ 13:30 pm. The emission peak started to weaken at around 15:30
366 pm ~ 16:00 pm and reached around zero or even turned into a small sink after 20:00 pm.

367 In summer, the Beilu'he site was a CH₄ sink of $-0.99 \pm 0.18 \text{ g CH}_4\text{-C m}^{-2} \text{ yr}^{-1}$
368 (Supplementary Figure 9 c), or $-13.28 \pm 0.38 \text{ mg CH}_4\text{-C m}^{-2} \text{ d}^{-1}$. The diel cycle of CH₄ fluxes in
369 summer was characterized with two absorption peaks and one small emission peak (Figure 4a3-
370 4e3). With T_{air} increasing after sunrise, the soil started to absorb atmospheric CH₄ and this soil
371 uptake process reached its first peak at around 9:30 am ~ 10:30 am. After that, the continuously
372 increasing T_{air} turned to suppress CH₄ uptake and promote CH₄ emissions, likely due to different
373 temperature sensitivities of methanotrophic and methanogenic bacteria. At around 15:30pm ~

374 16:00 pm, when T_{air} reached the maximum (Supplementary Figure 1b), CH_4 emission also
375 reached its peak. The following temperature decrease in the late afternoon again reversed the
376 CH_4 uptake / emission process, and by sunset we observed another CH_4 sink peak. The rate of
377 CH_4 sink then decreased again through the night with further decreasing temperature.

378 Autumn was another season with a net CH_4 sink, with the season having the highest
379 observed value for the site as a CH_4 sink in 2013 (Supplementary Figure 9d). The CH_4 sink in
380 autumn varied between $-0.69 \pm 0.19 \text{ g CH}_4\text{-C m}^{-2}$ (2015), and $-1.59 \pm 0.33 \text{ g CH}_4\text{-C m}^{-2}$ (2013),
381 with an average diel rate of $-1.19 \pm 0.48 \text{ g CH}_4\text{-C m}^{-2} \text{ yr}^{-1}$ or $-13.31 \pm 0.28 \text{ mg CH}_4\text{-C m}^{-2} \text{ d}^{-1}$.
382 The diel dynamics of autumn CH_4 fluxes was like a letter “V”, with a single sink peak during
383 13:30 pm \sim 15:30 pm (Figure 4a4-4e4).

384 **3.3 Response of Methane Fluxes to Changes in Environmental Factors**

385 Diel fluxes of CH_4 were correlated with many biotic and abiotic environmental factors,
386 either positively or negatively (Table 3). Positive factors include metagenomics of both
387 methanotrophic ($r = 0.52, p < 0.01$) and methanogens ($r = 0.49, p < 0.01$) at 0 – 25 cm soils,
388 ALT ($r = 0.43, p < 0.01$), and wind speed ($r = 0.15, p < 0.01$). Important negative factors include
389 VPD ($r = -0.26, p < 0.01$), SWC at all depths (varied r values between -0.17 and $-0.26, p < 0.01$),
390 T_{air} ($r = -0.11, p < 0.01$), and air pressure ($r = -0.15, p < 0.01$). The correlation signal between
391 CH_4 fluxes and T_{soil} changed with soil depths (varied r values between -0.09 and $0.24, p < 0.01$).
392 Furthermore, path analysis results showed that T_{soil} at 5cm and 10cm were the most important
393 factors, which together contributed about 25% of the relative importance coefficient. Following
394 these factors in importance were SWC at 80 cm (14%) and 20 cm (12%), and T_{soil} at 20 cm (8%).

395 Further analyses suggested that dominant control factors of CH₄ fluxes also changed
396 among different seasons. In spring, Rn was the most important factor, with a relative importance
397 coefficient near 60%, followed by SHF at 5 cm (9%), and SWC at 20 cm (6%). Table 4 shows
398 the results of the PCA. In spring, PC1 explained 63% of the CH₄ variations, which was
399 positively correlated with T_{air}, VPD, Rn, SHF of 15 cm, ALT, ΔI, SWC of 10 – 40 cm, T_{soil} of 0
400 cm, T_{soil} of 5 – 20 cm, T_{soil} of 30 – 50 cm, and negatively correlated with wind speed. The PC2
401 explained about 23% of CH₄ fluxes variations. The first four principal components explained
402 about 86% of the CH₄ variations.

403 In summer, CH₄ fluxes were mostly related with T_{soil} at 100 cm and 200 cm, with a
404 relative importance coefficient of about 30.2% and 26.5%, respectively. Other important
405 environmental determinants of CH₄ fluxes were T_{soil} at 70 cm (12.3%), and T_{soil} at 0 – 20 cm
406 (11.4%). The first four principal components explained about 88% of the CH₄ variations (Table
407 4). PC1 explained 70% of the CH₄ variations and was positively correlated with wind speed, T_{air},
408 VPD, SHF of 15 cm, ALT, ΔI, SWC of 50 – 160 cm, precipitation, T_{soil} of 0 cm, T_{soil} of 5 – 40
409 cm, T_{soil} of 50 – 80 cm, and T_{soil} of 100 – 200 cm, but negatively correlated with Rn and SWC of
410 10 – 40 cm.

411 In autumn, Rn and T_{soil} at 5 – 20 cm had the highest relative importance coefficients for
412 explaining the CH₄ flux variation. The first four principal components explained about 86% of
413 the CH₄ variations (Table 4). PC1 explained 69% of the CH₄ variations and was positively
414 correlated with T_{air}, VPD, Rn, SHF of 15 cm, ALT, ΔI, SWC of 10 – 40 cm, SWC of 50 – 160
415 cm, T_{soil} of 0 cm, T_{soil} of 5 – 40 cm, T_{soil} of 50 – 80 cm, and T_{soil} of 100 – 200 cm, but negatively
416 correlated with wind speed.

417 During winter, Rn was again the most important factor (34% relative importance
418 coefficient), followed by T_{soil} at 0 – 40 cm (27% in total), and SHF of 15 cm (17% in total), in
419 determining CH₄ fluxes. The first four principal components explained about 96% of the CH₄
420 variations (Table 4). PC1 explained 75% of the CH₄ variations and was positively correlated
421 with wind speed, T_{air}, VPD, Rn, SHF of 15 cm, ΔI, T_{soil} of 0 cm, and T_{soil} of 5 – 20 cm.

422 **3.4 Empirical Model Comparison for Different CH₄ Flux Season Classification System**

423 Lastly, we also compared how different season definitions, including the methods of
424 SMT, VCT, JMC, and VPC, may have impacted the predictability of CH₄ fluxes. We established
425 empirical maximum likelihood models between all environmental factors and diel CH₄ fluxes
426 over each season, and then compared modeled CH₄ fluxes and field observations under those
427 methods of different seasonal definitions (Figure 5). We found that the agreement between
428 modeled and observed CH₄ fluxes, using the new SMT method, reached $R^2 = 0.28$, almost twice
429 that of the VPC ($R^2 = 0.17$) and VCT ($R^2 = 0.14$) methods, and more than three times that of the
430 JMC method ($R^2 = 0.08$; Figure 5). Hence, the comparison suggested that our new method could
431 better model CH₄ fluxes over a year. The use of the traditional plant growing season versus
432 nongrowing season definitions may also underestimate or overestimate CH₄ sinks or sources,
433 especially when many studies assume CH₄ is close to zero during the plant nongrowing season.
434 Furthermore, the new SMT method accurately captures the impact of spring and autumn
435 permafrost thawing / freezing cycles on CH₄ fluxes, and the different preferable environments
436 for methanogens and methanotrophic bacteria during the summer season, while conventional
437 methods do not.

438 **4. Discussion**

439 **4.1 Annual, Season mean and Diel Variability**

440 Our results suggested that the alpine steppe ecosystem in Beilu'he was a CH₄ sink of
441 about $-0.86 \pm 0.23 \text{ g CH}_4 - \text{C m}^{-2} \text{ yr}^{-1}$ during the study period of 2012-2016. This sink strength is
442 larger than that of previous reports from other sites of the QTP (Cao et al., 2008; Wei et al.,
443 2012; Li et al., 2012; Song et al., 2015; Chang and Shi, 2015), and many other high-latitude
444 Arctic tundra ecosystems, like northeast Greenland (Jørgensen et al., 2015), western Siberia
445 (Liebner et al., 2011), and Alaska (Whalen et al., 1992; Zhuang et al., 2004; Whalen, 2005).
446 Different soil hydrothermal conditions, which previous studies have shown will greatly influence
447 CH₄ cycles in permafrost regions (Spahni et al., 2011; Kirschke et al., 2013), may partly explain
448 the site difference in CH₄ dynamics. For example, compared to the wet and often snow-covered
449 high-latitude Arctic tundra ecosystems, there is no or little snow cover during the cold season in
450 the QTP alpine steppes (Supplementary Table 1). During winter, the Beilu'he meteorological
451 data shows that the snow-cover time < 33.7h, SWC of 0-40cm within footprint < 7.6% from
452 2012 to 2016 (Supplementary Table 1), is far below high-latitude Arctic tundra ecosystems.
453 Jansson and Taş (2014) pointed out that relatively dry soils could facilitate the oxidation of CH₄,
454 since the increased number of gaps between soil particles in dry soils enhances the diffusion of
455 oxygen (O₂) and CH₄ molecules and promotes aerobic respiration of soil microorganisms (Wang
456 et al., 2014; Song et al., 2015). Meanwhile, unfrozen or capillary water found in cold-season
457 permafrost soils ensures sufficient soil moisture for microbial activities, even in relatively drier
458 and cold soils (Panikov and Dedysh, 2000; Rivkina et al., 2004). In addition, many previous
459 studies used static chambers in CH₄ measurements, and may not have included a plant non-
460 growing season (Wei et al., 2015a; Wang et al., 2014). Static chambers could underestimate CH₄

461 uptake because of the additional chamber heating-induced CH₄ emissions and frequent
462 measurement gaps from overheating preventive shutdowns (Sturtevant et al., 2012).

463 We argued that seasonal freezing and thawing dynamics may be a key reason to explain
464 the site's seasonal difference in CH₄ dynamics. Freezing and thawing processes are typical
465 characteristics of the QTP permafrost (Wang et al., 2008; Wang et al., 2000; Qin et al., 2016).
466 Our work suggests that freezing and thawing dynamics have played a critical role in governing
467 permafrost seasonal and diel CH₄ cycling. For instance, while both spring and autumn are active
468 seasons for the freeze-thaw dynamics of top soil layers and share many similarities, they have
469 opposite CH₄ processes—soils emit CH₄ during spring (Supplementary Figure 9 b), but consume
470 CH₄ during autumn (Supplementary Figure 9d). We hypothesize that the difference in the
471 freezing and thawing processes of the two seasons may have played a critical role in determining
472 the direction of CH₄ dynamics. In spring, the SWC of 10 cm, of 20-40 cm of 80 cm, and of 160
473 cm depth is 12.4%, 9.2%, 11.4%, and 13.6%, respectively (Supplementary Table 1). The active
474 soil layer thaws from top to bottom (Jin et al., 2000; Cao et al., 2017), and the permafrost table is
475 very shallow (about 10 ~ 45 cm) and often water proof (Wu and Zhang, 2008; Song et al., 2015;
476 Lin et al., 2015). The water thawed during the day time would freeze again at night on the soil
477 surface (Supplementary Figure 10a; Shi et al., 2006; Wu and Zhang, 2010b). The thin-ice layer
478 could stop atmospheric gases of CH₄ and O₂ from getting into the soils (Gazovic et al., 2010).
479 During autumn, the SWC is 15.3% at 10 cm below ground, decreases to 9.4% at 20-40 cm, and
480 then increases to 13.6% and 21.0% at 80 cm and 160 cm, respectively (Supplementary Table 1).
481 However, soils are bi-directionally frozen from both top (ground surface) and bottom
482 (permafrost table) which is about 200~400 cm below ground (Supplementary Figure 8; Wu and
483 Zhang, 2010a). On the one hand, the frozen soil of the ground surface (about 0-40cm) prevents

484 the outside liquid water from permeating. On the other hand, the freezing itself will reduce the
485 liquid water content in the soil. Therefore, it creates finely closed anaerobic gaps that allow CH₄
486 and O₂ gases into deep soils (about 50~400 cm; Mastepanov et al., 2008; Mastepanov et al.,
487 2013; Zona et al., 2016). Meanwhile, the temperature of deep soils (about 50~400 cm) still
488 remains at a relatively high level (Supplementary Figure 10b), and methanotrophic bacteria will
489 still be active at this high T_{soil} (Figure 2). This could be one important mechanism for autumn
490 soil CH₄ consumption. In addition, in principal it is also possible that the observed seasonal
491 variation in CH₄ flux may actually arise from the spatial variation of the footprint covered by the
492 eddy covariance site (within 175 m), given that prevalent wind direction changes seasonally
493 (Supplementary Figure 4). Nonetheless, we found that the same vegetation species and soil exist
494 in different directions to the tower within the footprint (Supplementary Figure 11). This spatial
495 vegetation and soil homogeneity rules out the potential influence of footprint changes on the sign
496 of CH₄ balances, and further confirms that seasonal soil freezing and thawing differences may
497 likely be the main explanation for seasonal CH₄ variations.

498 Furthermore, we suggested that the specific autumn soil vertical structure may help to
499 explain why the site was a CH₄ sink, unlike the CH₄ source in spring. The sequential probing
500 data enables us to establish a rough estimate on the soil vertical structure during the autumn
501 thawing–freezing process, in which the vertical distribution of clay, sandy soils, and soil organic
502 layers was mixed like a multi–layer hamburger structure, rather than forming a gradual change
503 (Figure 6e). As the soil profile is vertically different in features such as soil density, thermal
504 conductivity, latent heat, soil salinity, we boldly conjecture that the T_{soil}, SWC, and soil
505 microbial activities also had this hamburger type of vertical distribution in a similar way. As a
506 result, layers of frozen and thawed soils were not changing gradually but appeared like a

507 hamburger structure too. This soil vertical structure trapped high concentrations of soil water
508 between the frozen layers, which was therefore highly anaerobic and suitable for CH₄
509 production. It may also allow speculation that biogenic CH₄ between frozen layers could not
510 escape in autumn. The biogenic CH₄ would be trapped until the active soil layer was completely
511 frozen in late autumn, and in some warmer years until early winter and created frost cracks. This
512 would enable it to escape and may explain why there was a large burst of CH₄ emissions in late
513 autumn and early winter and may also explain the constantly weak CH₄ emission through the
514 winter season, although methanogenic bacteria may have stopped functioning in the low
515 temperature of winter. Of course, further studies and direct data collection in the field will be
516 needed to fully test the hypothesis.

517 **4.2 Impacts of Environmental, Permafrost, and Microbial Activities on CH₄ Fluxes**

518 Our results demonstrated the important roles of climate, freezing and thawing dynamics,
519 and soil microbe activities in regulating the direction and amount of CH₄ exchanges between the
520 atmosphere and ecosystems in permafrost areas. The key role of the above factors and processes
521 was also confirmed by the better representation of seasonal CH₄ cycles by our new seasonal
522 division method based on soil microbes, temperature, and permafrost dynamics rather than T_{air} or
523 vegetation phenology. Here, we further discuss potential mechanisms of how environmental
524 (including air and soil heat and water), freezing and thawing processes, and soil microbes control
525 the production and absorption of CH₄.

526 First, it is noteworthy that both the strength and direction of correlations between CH₄
527 fluxes, SWC, and T_{soil} parameters changed with soil depths, particularly during spring and
528 autumn, when active layer soils shifted between thawing and freezing regularly. The positive and
529 negative CH₄ flux correlations with T_{soil} and SWC may suggest that the impacts of T_{soil} and SWC

530 on CH₄ fluxes shall be treated as a holistic process (Table 3), rather than as separate ones. For
531 instance, in autumn, the significant correlation between CH₄ fluxes and T_{soil} or SWC was
532 positive at some soil depths, but negative at some other depths, reaching the maximum at the
533 depth of 80 cm. Further, *in situ* observations suggested that soil organic matter and soil microbe
534 amount were also at a very high level at this depth, highlighting that the regulation of soil abiotic
535 factors on CH₄ cycling may be well influenced by soil biotic activities. In addition, the holistic
536 soil heat–water process could also determine the concentration of soil inorganic ions, particularly
537 during spring and autumn, which were critical factors controlling the amount of soil unfrozen
538 water. Earlier studies suggested that soil unfrozen water is important for maintaining soil
539 microbial activities in winter (Panikov and Dedysh, 2000; Rivkina et al., 2004). In the future we
540 will include data acquiring of soil unfrozen water to test its role in regulating CH₄ exchanges in
541 permafrost regions.

542 T_{air} and precipitation impact CH₄ fluxes indirectly through their influences on T_{soil} and
543 SWC (Zhuang et al., 2004; Lecher et al., 2015). Such indirect influences may often be
544 characterized with time–lagged effects (Koven et al., 2011). For instance, post–drought rainfall
545 events in summer can first promote soil CH₄ consumption (summer of 2014). This is because
546 certain soil moisture is needed for methanogenic bacteria to function (Del et al., 2000; Luo et al.,
547 2012). Yet, prolonged rainfall will eventually cause CH₄ fluxes to change from negative (soils
548 consume CH₄) to positive (soils emit CH₄) fluxes (for example, day 168 to 183 of 2015, Figure
549 3d). After rainfall events, CH₄ flux gradually turned negative again with the decrease of SWC.
550 As a result of these time–lagged effects, the correlation coefficient between CH₄ fluxes and
551 precipitation often appears very low, although still statistically significant.

552 Second, soil methanogenic and methanotrophic bacteria could co-exist with different
553 optimal niches (e.g., ranges of $T_{\text{air}} / T_{\text{soil}}$ and SWC; Zhuang et al., 2013; Lau et al., 2015; Wei et
554 al., 2015a). For example, the CH_4 diel cycle in summer was found to have two strong
555 consumption peaks and one weak emission peak (Figure 4: a3, c3, d3, e3). The timing of these
556 different peaks may well reflect the different environmental requirements for the dominance of
557 methanogens and methanotrophic bacteria. Furthermore, methanogens may have a broader
558 functional temperature range than methanotrophic bacteria (Kolb, 2009; Lau et al., 2015; Yang et
559 al., 2016). This is also evident, for example, from the diel CH_4 cycle in autumn when CH_4
560 consumption was minimal at both lowest and highest T_{air} (Figure 4a4-4e4).

561 The complex relationships between CH_4 fluxes and environmental factors make it a grand
562 challenge to predict the future of the QTP CH_4 budget under a changing climate. For instance, it
563 has been generally believed that the ALT will increase under projected warming (Wu and Liu,
564 2004). The positive correlation between CH_4 fluxes and ALT found here suggests that the QTP
565 permafrost CH_4 sink may thus be weakened. However, the negative correlation between CH_4
566 flux and T_{air} may lead to a different conclusion. Incorporating our findings and high-resolution
567 data into mechanistic CH_4 models is therefore needed to enhance our capacity in predicting
568 future CH_4 budgets. Earth system models have been introduced to estimate CH_4 dynamics
569 (Curry, 2007; Spahni et al., 2011; Bohn et al., 2015). For example, using a terrestrial ecosystem
570 modelling approach, Zhuang et al. (2004) estimated the average QTP permafrost CH_4 sink of -
571 $0.08 \text{ g C m}^{-2} \text{ yr}^{-1}$, much smaller than our field-based CH_4 estimate ($-0.86 \pm 0.23 \text{ g CH}_4\text{-C m}^{-2} \text{ yr}^{-1}$).
572 Current CH_4 models focus on the regulation of CH_4 processes by temperature and SWC, and
573 usually lack high-resolution data for model parameterization (Bohn et al., 2015). Data
574 interpolation and the use of average values of certain environmental factors are normal practices

575 in most models (Zhuang et al., 2004), which may overlook the impacts of environmental
576 variations on CH₄ dynamics. For example, at Beilu'he, T_{air} on a typical summer day (e.g., July
577 6th, 2013) could vary between -6 °C and 28 °C, a difference of 34 °C. The resulting diel mean
578 temperature, 17 °C, is beyond the range of methanotrophic bacteria's preferable temperature of
579 20~30 °C (Segers, 1998; Steinkamp et al., 2001; Yang et al., 2016). Therefore, models using
580 diel mean temperature as an input may estimate the site as a net CH₄ sink. However, field
581 observations show a source with a sink only during a short period (8:30am~11:30 am), on July
582 6th, 2013, because the short period of the sink was offset by the source over the remaining 21
583 hours.

584 Furthermore, half-hourly SWC was well related with the waterproof role by the
585 permafrost layer during spring and autumn (Figure 6a). However, because of the shortage of high
586 temporal resolution data, half-diel or diel mean SWC data are often used in many previous
587 studies (Zhu et al., 2004; Jiang et al., 2010; Wei et al., 2015b), which could not correctly show
588 the regulation of permafrost soil properties that are critical for CH₄ dynamics. As another
589 example, T_{soil} of 0 – 50 cm depth is one of the most important factors related to CH₄ fluxes
590 (Mastepanov et al., 2008). However, many studies used T_{air} or re-analyzed deep T_{soil} instead
591 (Zhu et al., 2004; Bohn et al., 2015; Oh et al., 2016). Because the active layer is not
592 homogeneous, but with different thermal conductivities during the freezing and thawing process,
593 the use of T_{air} or deep T_{soil} brings in large uncertainties in CH₄ modelling. Future research needs
594 to improve mechanistic understanding of CH₄ dynamics and their biotic and abiotic control
595 factors, and to conduct more high-resolution and long-term field monitoring.

596 **4.3 The Classification System of the Four Seasons for CH₄ Studies**

597 Our study differs also from the majority of earlier studies regarding the definition of the
598 seasons (Treat et al., 2014; Wang et al., 2014; Wei et al., 2015a; Song et al., 2015). Here, we
599 adopted a new classification system of the four seasons based on 0 – 25 cm soil depth bacterial
600 activities (Figure 2), T_{soil} of 0 – 40 cm (Supplementary Figure 6a), and ALT (Supplementary
601 Figure 8), rather than the conventional methods based on T_{air} and vegetation dynamics (Chen et
602 al., 2011; McGuire et al., 2012). Previous studies indicated that changes in CH₄ fluxes are
603 regulated by soil microbes, and activities of soil microbes are not limited to the warm season
604 (Zhuang et al., 2004; Lau et al., 2015; Yang et al., 2016). For instance, in March and November,
605 we found the amount of gene expression by methanogens and methanotrophs at 0 – 25 cm soils
606 were about 16.8% and 35.6% (Figure 2), respectively, suggesting there are still strong microbial
607 activities during the cold and dry season. Therefore, our new method of defining the four seasons
608 from the top soil biotic and abiotic features better captures the pattern of CH₄ dynamics
609 throughout a year.

610 **5. Conclusions**

611 Our field data indicates that there was a large CH₄ sink in the QTP permafrost area during
612 recent years. The strength of this CH₄ sink is larger than found in previous studies in the same
613 region and many high-latitude tundra ecosystems. This study highlights the complexity of
614 environmental controls, including soil heat-water processes, permafrost freezing and thawing
615 dynamics, and soil microbial activities, on CH₄ cycling. This complexity implies that linear
616 interpolation and extrapolation from site-level studies could introduce large uncertainties in CH₄
617 flux estimation. Future quantification of CH₄ dynamics in permafrost regions needs to account
618 for the effects of complex environmental processes. Our findings also highlight the importance

619 of conducting more high-resolution and long-term field monitoring in permafrost regions for
620 better understanding and modelling of permafrost CH₄ cycling under a changing climate.

621 **Acknowledgements**

622 We would like to thank Yongzhi Liu, Jing Luo, Ji Chen, Guilong Wu, Wanan Zhu, Zhipeng
623 Xiao, and Chang Liao for their tremendous help in collecting field data over all these years. We
624 also want to pay tribute and gratitude to the late Xiaowen Cui for his contribution to our many
625 field adventures. We thank John McCabe for proofreading the manuscript. This study was
626 supported by the National Natural Science Foundation of China (41501083), Key Research
627 Program of Frontier Sciences, Chinese Academy of Sciences (QYZDJ-SSW-DQC011), Opening
628 Research Foundation of Key Laboratory of Land Surface Process and Climate Change in Cold
629 and Arid Regions, Chinese Academy of Sciences (LPCC201307), and Opening Research
630 Foundation of Plateau Atmosphere and Environment Key Laboratory of Sichuan Province
631 (PAEKL – 2014 – C3). A. C. acknowledges the support from a Purdue University Forestry and
632 Natural Resources research scholarship. The data generated in this study will be freely available
633 on the Asia Flux regional network server (<https://db.cger.nies.go.jp/asiafluxdb/>).

634 **Reference**

- 635 Bohn T., Melton J., Ito A.: WETCHIMP–WSL: intercomparison of wetland methane emissions
636 models over West Siberia, *Biogeosciences*, 12, 3321 – 3349, 2015.
- 637 Burba, G. G., Mcdermitt, D. K., and Grelle, A.: Addressing the influence of instrument surface
638 heat exchange on the measurements of CO₂ flux from open-path gas
639 analyzers. *Glob. Change Biol.*, 14(8), 1854 – 1876, 2008.
- 640 Cao G., Xu X., and Long R.: Methane emissions by alpine plant communities in the Qinghai–

641 Tibet Plateau, *Biol. Lett.*, 4, 681 – 684, 2008.

642 Cao B., Gruber S., Zhang T.: Spatial variability of active layer thickness detected by ground–
643 penetrating radar in the Qilian Mountains, Western China, *J. Geophys. Res. Earth Surf.*,
644 122, 574 – 591, 2017.

645 Cate, R. B., and Nelson, L. A.: A simple statistical procedure for partitioning soil test correlation
646 data into two classes, *Soil Sci. Soc. Am. J.*, 35(4), 658 – 660, 1971.

647 Chang R., Miller C., and Dinardo S.: Methane emissions from Alaska in 2012 from CARVE
648 airborne observations, *Proc. Natl. Acad. Sci. U. S. A.*, 111, 16694 – 16699, 2014.

649 Chang S. and Shi P.: A review of research on responses of leaf traits to climate change, *Chin. J.*
650 *Plant Ecol.*, 39, 206 – 216, 2015.

651 Chen W., Wolf B., and Zheng X.: Annual methane uptake by temperate semiarid steppes as
652 regulated by stocking rates, aboveground plant biomass and topsoil air permeability.
653 *Glob. Change Biol.*, 17, 2803 – 2816, 2011.

654 Curry C.: Modeling the soil consumption at atmospheric methane at the global scale. *Glob.*
655 *Biogeochem. Cycles*, 21, 1 – 15, 2007.

656 Dengel S., Zona D., and Sachs T.: Testing the applicability of neural networks as a gap–filling
657 method using CH₄ flux data from high latitude wetlands. *Biogeosciences*, 10, 8185 – 8200,
658 2013.

659 Del G., Parton W., and Mosier A.R.: General CH₄ oxidation model and comparisons of CH₄
660 oxidation in natural and managed systems, *Glob. Biogeochem. Cycles*, 14, 999 – 1019,
661 2000.

662 Falge, E., Baldocchi, D., and Olson, R.: Gap filling strategies for defensible annual sums of net
663 ecosystem exchange, *Agric. For. Meteorol.*, 107(1), 43 – 69, 2001.

664 Gažovič M., Kutzbach L., and Schreiber P.: Diurnal dynamics of CH₄ from a boreal peatland
665 during snowmelt. *Tellus, B*, 62, 133 – 139, 2010.

666 IPCC, climate change 2013: the physical science basis. Contribution of working group I to the
667 fifth assessment report of the intergovernmental panel on climate change., 2013.

668 Jansson, J. K. and Tas, N.: The microbial ecology of permafrost, *Nat. Rev. Microbiol.*, 12, 414,
669 2014.

670 Jiang C., Yu G., and Fang H.: Short-term effect of increasing nitrogen deposition on CO₂, CH₄
671 and N₂O fluxes in an alpine meadow on the Qinghai–Tibetan Plateau, China, *Atmos.*
672 *Environ.*, 44, 2920 – 2926, 2010.

673 Jin H., Li S., and Cheng G.: Permafrost and climatic change in China, *Glob. Planet, Change*, 26,
674 387 – 404, 2000.

675 Jørgensen, C. J., Johansen, K. M. L., and Westergaard–Nielsen, A.: Net regional methane sink in
676 High Arctic soils of northeast Greenland, *Nat. Geosci.*, 8, 20, 2015.

677 Kirschke, S., Bousquet, P., and Ciais, P.: Three decades of global methane sources and
678 sinks, *Nat. Geosci.*, 6, 813, 2013.

679 Kolb, S.: The quest for atmospheric methane oxidizers in forest soils, *Environ. Microbiol.*
680 *Rep.*, 1, 336 – 346, 2009

681 Koven C.D., Ringer B., and Friedlingstein P.: Permafrost carbon–climate feedbacks accelerate
682 global warming, *Proc. Natl. Acad. Sci. U. S. A.*, 108, 14769 – 14774, 2011.

683 Lau M., Stackhouse B.T., and Layton A.C.: An active atmospheric methane sink in high Arctic
684 mineral cryosols. *ISME J.*, 9, 1880 – 1891, 2015.

685 Lecher A.L., Dimova N., and Sparrow K.J.: Methane transport from the active layer to lakes in
686 the Arctic using Toolik Lake, Alaska, as a case study, *Proc. Natl. Acad. Sci. U. S. A.*, 112,
687 3636 – 3640, 2015.

688 Lee, X., Massman, W., and Law, B. (Eds.): *Handbook of micrometeorology: a guide for surface*
689 *flux measurement and analysis (Vol. 29)*, Springer Science and Business Media, 2006.

690 Li K., Gong Y., and Song W.: Responses of CH₄, CO₂ and N₂O fluxes to increasing nitrogen
691 deposition in alpine grassland of the Tianshan Mountains, *Chemosphere*, 88, 140 – 143,
692 2012.

693 Liebner S., Zeyer J., and Wagner D.: Methane oxidation associated with submerged brown
694 mosses reduces methane emissions from Siberian polygonal tundra, *J. Ecol.*, 99, 914 – 922,
695 2011.

696 Lin Z., Burn C.R., and Niu F.: The Thermal Regime, including a Reversed Thermal Offset, of
697 Arid Permafrost Sites with Variations in Vegetation Cover Density, Wudaoliang Basin,
698 Qinghai–Tibet Plateau. *Permafr. Periglac. Process.*, 26, 142 – 159, 2015.

699 Loescher, H. W., Law, B. E., and Mahrt, L: Uncertainties in, and interpretation of, carbon flux
700 estimates using the eddy covariance technique. *J. Geophys. Res. Atmos.*, 111(D21), 2006.

701 Luo G.J., Brüggemann N., and Wolf B.: Decadal variability of soil CO₂, NO, N₂O, and CH₄
702 fluxes at the Höglwald Forest, Germany. *Biogeosciences*, 9, 1741 – 1763, 2012.

703 Mastepanov M., Sigsgaard C., and Dlugokencky E.J.: Large tundra methane burst during onset

704 of freezing. *Nature*, 456, 628 – 30, 2008.

705 Mastepanov, M., Sigsgaard, C., and Tagesson, T.: Revisiting factors controlling methane
706 emissions from high-Arctic tundra, *Biogeosciences*, 10(7), 5139, 2013.

707 Mauder, M., Cuntz, M., and Drüe, C.: A strategy for quality and uncertainty assessment of long–
708 term eddy–covariance measurements. *Agric. For. Meteorol.*, 169, 122 – 135, 2013.

709 McGuire A.D., Christensen T.R., and Hayes D.: An assessment of the carbon balance of Arctic
710 tundra: Comparisons among observations, process models, and atmospheric inversions,
711 *Biogeosciences*, 9, 3185 – 3204, 2012.

712 Moncrieff, J., Clement, R., and Finnigan, J.: Averaging, detrending, and filtering of eddy
713 covariance time series. In *Handbook of micrometeorology* (pp. 7 – 31), Springer
714 Netherlands, 2004.

715 Muller, S. W. *Permafrost or permanently frozen ground and related engineering problems*, 1947.

716 Oh Y., Stackhouse B., and Lau M.: A scalable model for methane consumption in arctic mineral
717 soils. *Geophys. Res. Lett.*, 43, 5143 – 5150, 2016.

718 Panikov N.S. and Dedysh S.N.: Cold season CH₄ and CO₂ emission from boreal peat bogs (West
719 Siberia): Winter fluxes and thaw activation dynamics, *Glob. Biogeochem. Cycles*, 14, 1071
720 – 1080, 2000.

721 Papale, D., Reichstein, M., and Aubinet, M.: Towards a standardized processing of Net
722 Ecosystem Exchange measured with eddy covariance technique: algorithms and uncertainty
723 estimation. *Biogeosciences*, 3(4), 571 – 583, 2006.

724 Patra P.K. and Kort E.A.: Regional Methane Emission Estimation Based on Observed

725 Atmospheric Concentrations (2002 – 2012), *J. Meteor. Soc. Japan. Ser. II*, 94, 91 – 113,
726 2016.

727 Qin, Y., Wu T., and Li R., Using ERA-Interim reanalysis dataset to assess the changes of ground
728 surface freezing and thawing condition on the Qinghai–Tibet Plateau. *Environ. Earth Sci.*,
729 75(9): 1-13, 2016.

730 Rigby M., Prinn R.G., and Fraser P.J.: Renewed growth of atmospheric methane, *Geophys. Res.*
731 *Let.*, 35, 2 – 7, 2008.

732 Rivkina E., Laurinavichius K., and McGrath J.: Microbial life in permafrost, *Adv. Space Res.*,
733 33, 1215 – 1221, 2004.

734 Segers R.: Methane production and methane consumption—a review of processes underlying
735 wetland methane fluxes [Review], *Biogeochem.*, 41, 23 – 51, 1998.

736 Shi P., Sun X., and Xu L.: Net ecosystem CO₂ exchange and controlling factors in a steppe–
737 Kobresia meadow on the Tibetan Plateau. *Sci. China Ser. D-Earth Sci.*, 49, 207 – 218, 2006.

738 Song, W., Wang, H., and Wang, G.: Methane emissions from an alpine wetland on the Tibetan
739 Plateau: Neglected but vital contribution of the non–growing season, *J. Geophys. Res.*
740 *Biogeosci.*, 120, 1475 – 1490, 2015.

741 Spahni R., Wania R., and Neef L.: Constraining global methane emissions and uptake by
742 ecosystems. *Biogeosciences*, 8, 1643 – 1665, 2011.

743 Steinkamp R., Butterbach–Bahl K., and Papen H.: Methane oxidation by soils of an N limited
744 and N fertilized spruce forest in the Black Forest, Germany, *Soil. Biol. Biochem.*, 33, 145 –
745 153, 2001.

- 746 Sturtevant C.S., Oechel W.C., and Zona D.: Soil moisture control over autumn season methane
747 flux, Arctic Coastal Plain of Alaska, *Biogeosciences*, 9, 1423 – 1440, 2012.
- 748 Treat C.C., Wollheim W.M., and Varner R.K.: Temperature and peat type control CO₂ and CH₄
749 production in Alaskan permafrost peats, *Glob. Chang. Biol.* 20, 2674 – 2686, 2014.
- 750 Vickers, D., and Mahrt, L.: Quality control and flux sampling problems for tower and aircraft
751 data. *J. Atmos. Ocean. Technol.*, 14(3), 512 – 526, 1997.
- 752 Wang G., Li Y., and Wang Y.: Effects of permafrost thawing on vegetation and soil carbon pool
753 losses on the Qinghai–Tibet Plateau, China, *Geoderma*, 143, 143 – 152, 2008.
- 754 Wang S., Jin H., Li S.: Permafrost degradation on the Qinghai–Tibet Plateau and its
755 environmental impacts. *Permafr. Periglac. Process.*, 11, 43 – 53, 2000.
- 756 Wang Y., Liu H., and Chung H.: Non–growing season soil respiration is controlled by freezing
757 and thawing processes in the summer monsoon-dominated Tibetan alpine grassland. *Glob.*
758 *Biogeochem. Cycles*, 28, 1081 – 1095, 2014.
- 759 Webb E. K., Pearman G. I., and Leuning R.: Correction of flux measurements for density effects due to
760 heat and water vapor transfer. *Q. J. Royal Meteorol. Soc.*, 106, 85 – 100, 1980.
- 761 Wei D., Ri X., and Wang Y.: Responses of CO₂, CH₄ and N₂O fluxes to livestock enclosure in an
762 alpine steppe on the Tibetan Plateau, China. *Plant Soil*, 359, 45 – 55, 2012.
- 763 Wei D., Ri X., and Tarchen T.: Considerable methane uptake by alpine grasslands despite the
764 cold climate: In situ measurements on the central Tibetan Plateau, 2008 – 2013, *Glob.*
765 *Chang Biol.*, 21, 777 – 788, 2015a.
- 766 Wei D., Tarchen T., and Dai D.: Revisiting the role of CH₄ emissions from alpine wetlands on

767 the Tibetan Plateau: Evidence from two in situ measurements at 4758 and 4320 m above sea
768 level, *J. Geophys. Res. Biogeosci.*, 120, 1741 – 1750, 2015b.

769 Whalen, S. C. and Reeburgh, W. S.: Consumption of atmospheric methane by tundra
770 soils. *Nature*, 346, 160, 1990.

771 Whalen S.C.: Biogeochemistry of Methane Exchange between Natural Wetlands and the
772 Atmosphere. *Environ. Eng. Sci.*, 22, 73 – 94, 2005.

773 Whalen S.C., Reeburgh W.S., and Barber V.A.: Oxidation of methane in boreal forest soils: a
774 comparison of seven measures. *Biogeochemistry*, 16, 181 – 211, 1992.

775 Wilson K., et al.: Energy balance closure at FLUXNET sites. *Agr Forest Meteorol.*, 113: 223-
776 243, 2002.

777 Wu Q. and Liu Y.: Ground temperature monitoring and its recent change in Qinghai–Tibet
778 Plateau, *Cold Reg. Sci. Technol.*, 38, 85 – 92, 2004.

779 Wu Q. and Zhang T.: Recent permafrost warming on the Qinghai–Tibetan Plateau. *J. Geophys.*
780 *Res. Atmos.* 113, 1 – 22, 2008.

781 Wu Q. and Zhang T.: Changes in active layer thickness over the Qinghai–Tibetan Plateau from
782 1995 to 2007, *J. Geophys. Res. Atmos.*, 115, D09107, 2010a.

783 Wu Q. Zhang T., and Liu Y.: Permafrost temperatures and thickness on the Qinghai–Tibet
784 Plateau, *Glob. Planet. Change*, 72, 32 – 38, 2010b.

785 Yang S., Wen X., and Shi Y.: Hydrocarbon degraders establish at the costs of microbial richness,
786 abundance and keystone taxa after crude oil contamination in permafrost environments. *Sci.*
787 *Rep.*, 6, 37473, 2016.

788 Zhu X., Zhuang Q., and Chen M.: Net exchanges of methane and carbon dioxide on the
789 Qinghai–Tibetan Plateau from 1979 to 2100. *Environ. Res. Lett.*, 10, 85007. 2004.

790 Zhuang Q., Melillo J.M., and Kicklighter D.W.: Methane fluxes between terrestrial ecosystems
791 and the atmosphere at northern high latitudes during the past century: A retrospective
792 analysis with a process–based biogeochemistry model. *Glob. Biogeochem. Cycles*, 18(3),
793 2004.

794 Zhuang Q., Chen M., and Xu K.: Response of global soil consumption of atmospheric methane
795 to changes in atmospheric climate and nitrogen deposition. *Glob. Biogeochem. Cycles*, 27,
796 650 – 663, 2013.

797 Zona D., Gioli B., and Commane R.: Cold season emissions dominate the Arctic tundra methane
798 budget. *Proc. Natl. Acad. Sci. U. S. A.*, 113, 40 – 45, 2016.

799

800

801

802

803

804

805

806

807

808 **Table 1.** Soil characteristics at the eddy covariance flux study site

Soil depth cm	Soil type	Gravel content g kg ⁻¹	SOC g kg ⁻¹	Microbial Numbers ×10 ⁴	pH	DBD g cm ⁻³	SWC %	Total N ×10 ³ mg kg ⁻¹
0 – 20	clay	22.3	2.8	3.44	8.7	1.75	18.26	0.87
20 – 50	silty clay	12.6	1.7	3.82	8.4	1.73	11.52	1.02
50 – 120	silt and fine sand	3.4	1.3	3.67	8.4	1.72	12.57	1.18
120 – 160	silt and fine sand	2.8	26.4	5.44	5.1	1.68	24.69	2.46
160 – 200	silt and fine sand	1.6	13.6	4.39	6.8	1.68	22.45	2.03

809 **Note:** Gravel content diameter ≥ 0.5cm. SOC is soil organic content, DBD is dry bulk density,
 810 SWC is soil water content, and Total N is total nitrogen content.

811

Table 2. Measurements of four seasons from 2012 to 2016

	Spring	Summer	Autumn	Winter	Plant growing season	Plant non-growing season
	Period; Total days	Period; Total days	Period; Total days	Period; Total days	Period; Total days	Period; Total days
	Days	Days	Days	Days	Days	Days
2012	50 – 142; 93	143 – 229; 87	230 – 323; 94	1 – 49, 324 – 366; 92	139 – 286; 148 ^a	1 – 138, 287 – 366; 218 ^a
					122 – 305; 184 ^b	1 – 121, 306 – 366; 182 ^b
					143 – 290; 148 ^c	1 – 142, 291 – 366; 218 ^c
2013	36 – 137; 102	138 – 224; 87	225 – 334; 110	1 – 35, 335 – 365; 66	139 – 287; 149 ^a	1 – 138, 288 – 365; 216 ^a
					121 – 304; 184 ^b	1 – 120, 305 – 365; 181 ^b
					127 – 297; 171 ^c	1 – 126, 298 – 365; 194 ^c
2014	49 – 127; 79	128 – 228; 101	229 – 309; 81	1 – 48, 310 – 365; 104	137 – 288; 152 ^a	1 – 136, 289 – 365; 213 ^a
					121 – 304; 184 ^b	1 – 120, 305 – 365; 181 ^b
					142 – 294; 153 ^c	1 – 141, 295 – 365; 212 ^c
2015	36 – 150; 115	151 – 224; 74	225 – 312; 88	1 – 35, 313 – 365; 88	145 – 288; 144 ^a	1 – 144, 289 – 365; 221 ^a
					121 – 304; 184 ^b	1 – 120, 305 – 365; 181 ^b
					136 – 295; 160 ^c	1 – 135, 296 – 365; 205 ^c
2016	47 – 161; 115	162 – 225; 64	226 – 299; 74	1 – 46, 300 – 366; 113	141 – 287; 147 ^a	1 – 140, 288 – 366; 219 ^a
					122 – 305; 183 ^b	1 – 120, 305 – 366; 182 ^b
					140 – 296; 157 ^c	1 – 139, 297 – 366; 209 ^c

813 **Note:** ^a, based on vegetation cover and temperature change (VCT) (Lund et al., 2010; Tang and Arnone, 2013; Song et al., 2015); ^b, based on Julian
814 months (JMC) (Da et al., 2015); ^c, based on vegetation phenology change (VPC). Spring , Summer, Autumn, Winter are based on parameters of
815 microbial activities, ALT variety coefficient and T_{soil} (SMT).

816

817

818

819

820

821

822

823

824

825

826

827

Table 3. Correlation coefficients between CH₄ fluxes and environment factors on half-hour time scales

Environment Factors	CH ₄ Flux									
	Spring		Summer		Autumn		Winter		2012 – 2016	
	r	n	r	n	r	n	r	n	r	n
T _{air}	0.25**	24144	0.14**	19818	-0.16**	20959	0.32**	22224	-0.11**	87145
Wind Speed	0.31**	24144	-0.04**	19817	-0.20**	20959	0.32**	22224	0.15**	87144
VPD	-0.33**	18624	-0.21**	19263	-0.09**	16737	-0.21	18000	0.26**	69624
Rn	0.55**	24143	0.09**	19807	-0.33**	20913	0.51**	22224	0.09**	87087
Albedo	0.07**	24144	-0.01	19814	-0.08**	20913	0.10**	22224	0.02**	87095
SHF of 5cm	0.46**	24144	-0.08**	19818	-0.23**	20913	0.43**	22224	0.09**	87099
SHF of 15cm	0.36**	24144	-0.15**	19815	-0.23**	20913	0.33**	22224	0.08**	87096
SWC of 10cm	-0.16**	24144	-0.14**	19818	-0.06**	20959	0.00	22224	-0.25**	87145
SWC of 20cm	-0.15**	24144	-0.13**	19816	-0.07**	20959	0.11**	22224	-0.24**	87143
SWC of 40cm	-0.11**	24144	-0.02**	19818	0.07**	20959	0.06**	22224	-0.17**	87145
SWC of 80cm			-0.13**	19818	0.06**	20959				
SWC of 160cm			0.04**	19818	-0.11**	20959				
Precipitation			-0.02	16748	0.01 ^b	17888				
ALT	0.73**	23004	0.23**	19823	0.73**	21454			0.43**	64281

ΔI	0.77**	100	0.57**	83	0.46**	89	0.23	93	0.49**	365
ΔII	0.31**	100	0.66**	83	0.78**	89	0.19	93	0.52**	365
T _{soil} of 0 cm	-0.06*	23004	0.13**	19823	0.07**	20366	0.13**	21711	0.11**	84904
T _{soil} of 5 cm	0.15**	24144	0.15**	19808	-0.13**	21454	0.27**	22224	0.24**	87630
T _{soil} of 10 cm	-0.03**	24144	0.12**	19808	0.08**	21454	0.16**	22224	0.13**	87630
T _{soil} of 20 cm	-0.14**	24144	0.08**	19808	0.02**	21454	0.06**	22224	-0.09**	87630
T _{soil} of 30 cm	-0.13**	23004	0.06**	19823	-0.02**	20366	0.07**	21711	-0.08**	84904
T _{soil} of 40 cm	0.14**	24144	0.05**	19808	-0.01 ^b	21454	0.06**	22224	0.11**	87630
T _{soil} of 50 cm			0.04**	19823	-0.05**	20366				
T _{soil} of 70 cm			0.07**	19823	-0.05**	20366				
T _{soil} of 80 cm			0.05**	19808	0.04**	21454				
T _{soil} of 100 cm			0.10**	19823	-0.05**	21454				
T _{soil} of 150 cm			0.09**	19823	-0.04**	20366				
T _{soil} of 160 cm			0.10**	19808	0.01**	21454				
T _{soil} of 200 cm			0.02**	19823	-0.02**	20366				

829 **Note:** ** means $p < 0.01$, * means $p < 0.05$; r values for the relationship between CH₄ flux and environment factors. T_{air} means air temperature of 3 m
830 above the ground surface. VPD is vapor pressure deficit, NR is net radiation, and SWC is soil water content, ALT is active layer thickness, which fitted
831 through the depth of soil 0 °C in Surfer 8.0., and the data is removed as meaningless in winter. T_{soil} is the temperature of the soil. In spring and winter,

832 precipitation data is too sparse for statistical analysis. ΔI is the soil 0 – 25cm archaeal methanogens gene expression, and ΔII is the soil 0 – 25 cm
833 methanotrophic gene expression. The coefficients (r) between CH_4 flux and ΔI , ΔII are obtained using the synchronous CH_4 fluxes averaged for 5 days.

834

835

836

837

838

839

840

841

842

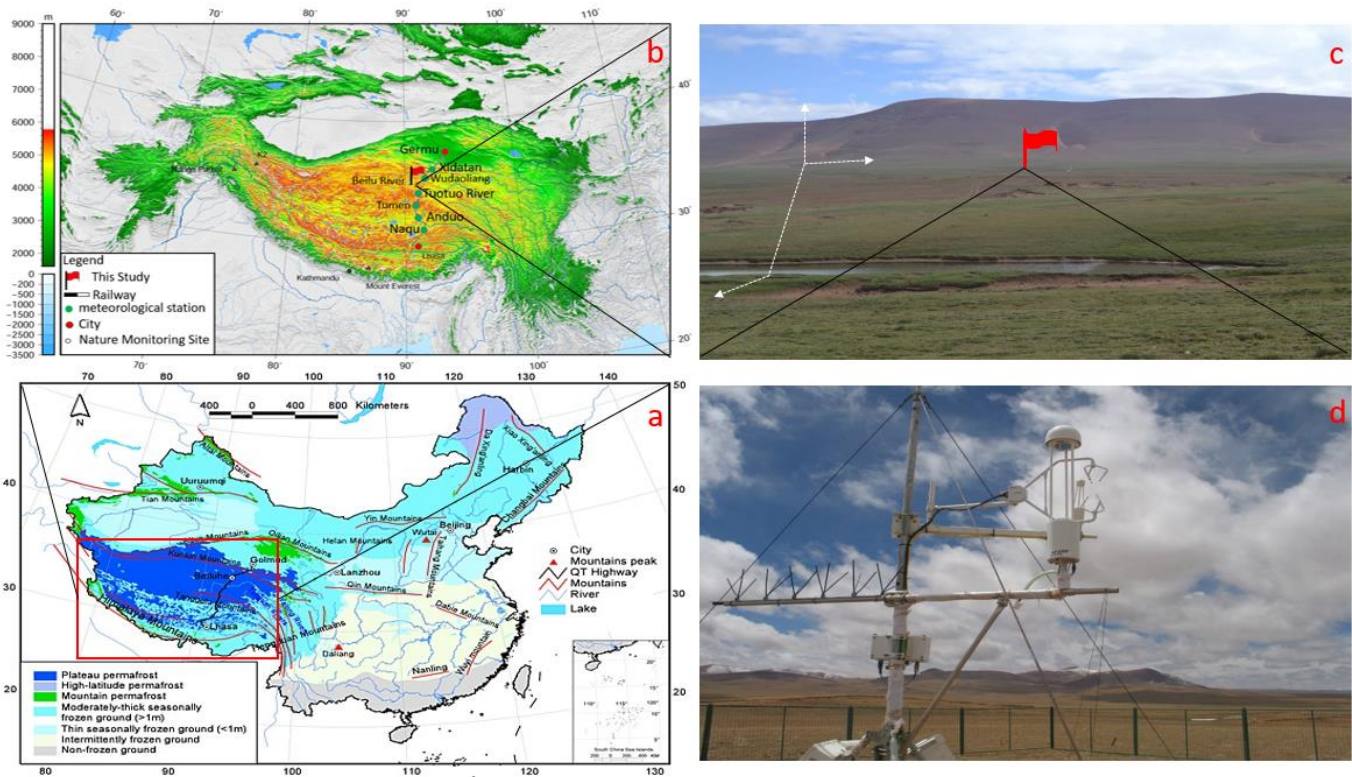
843

844

845 **Table 4.** Principal components analysis (PCA) of the environmental factors.

Component	Spring				Summer				Autumn				Winter			
	PC1	PC2	PC3	PC4	PC1	PC2	PC3	PC4	PC1	PC2	PC3	PC4	PC1	PC2	PC3	PC4
wind speed	-0.03	0.51	0.65	-0.46	0.02	0.37	0.38	-0.13	-0.04	0.44	0.59	0.67	0.27	0.45	-0.11	-0.27
T _{air}	0.38	0.29	-0.05	-0.11	0.42	0.22	-0.03	0.02	0.36	0.21	0.08	-0.06	0.48	0.12	-0.02	0.01
VPD	0.34	-0.27	0.40	0.15	0.17	0.46	-0.22	0.09	0.34	-0.15	0.17	-0.07	0.14	-0.15	0.95	-0.22
Rn	0.16	0.49	0.00	0.76	-0.01	0.07	0.58	0.11	0.12	0.54	-0.43	-0.07	0.26	0.47	-0.01	-0.49
SHF of 15cm	0.24	0.49	-0.30	-0.09	0.25	0.53	-0.09	0.01	0.15	0.59	-0.23	-0.15	0.36	0.37	0.14	0.58
ALT	0.22	-0.40	0.40	0.27	0.32	-0.53	-0.05	0.02	0.29	0.49	0.70	0.25				
ΔI	0.49	-0.22	0.01	-0.08	0.50	-0.16	0.02	-0.16	0.29	0.31	0.24	-0.51	0.52	0.05	0.07	-0.03
SWC of 10 – 20cm													-0.31	0.45	0.22	0.47
SWC of 10 – 40cm	0.33	-0.20	0.50	0.25	-0.16	0.15	-0.16	0.73	0.28	-0.18	-0.41	0.53				
SWC of 50 – 160cm					0.23	-0.20	-0.16	0.55	0.31	-0.17	-0.32	0.41				
Precipitation					0.03	-0.04	0.63	0.35								
T _{soil} of 0 cm	0.43	-0.07	-0.20	-0.27	0.43	0.08	0.08	-0.07	0.37	0.07	0.19	-0.16	0.43	-0.35	-0.15	0.09
T _{soil} of 5 – 20 cm	0.44	-0.01	-0.17	-0.16									0.45	-0.28	0.00	0.28
T _{soil} of 5 – 40 cm					0.46	-0.05	0.04	-0.03	0.38	0.02	0.18	-0.17				
T _{soil} of 30 – 50cm	0.40	-0.23	-0.08	-0.04												
T _{soil} of 50 – 80cm					0.37	-0.36	0.00	0.01	0.37	-0.11	0.19	-0.14				
T _{soil} of 100 – 200cm					0.33	-0.34	0.01	-0.01	0.36	-0.14	0.08	0.00				
Percent of variance	0.63	0.23	0.08	0.04	0.70	0.18	0.07	0.02	0.69	0.17	0.08	0.04	0.75	0.21	0.02	0.01
Cumulative	0.63	0.86	0.94	0.98	0.70	0.88	0.95	0.97	0.69	0.86	0.94	0.98	0.75	0.96	0.98	0.99

846 **Note:** PC means principal component. Before PCA, SWC was divided for three parts, 10 – 20 cm, 10 – 40 cm, and 50 – 160 cm according to collinearity
847 test in four seasons. T_{soil} was divided for six parts of T_{soil} of 0 cm, T_{soil} of 5 – 20 cm, T_{soil} of 5 – 40 cm, T_{soil} of 30 – 50 cm, T_{soil} of 50 – 80 cm, and T_{soil}
848 of 60 – 200 cm according to collinearity test in different seasons.

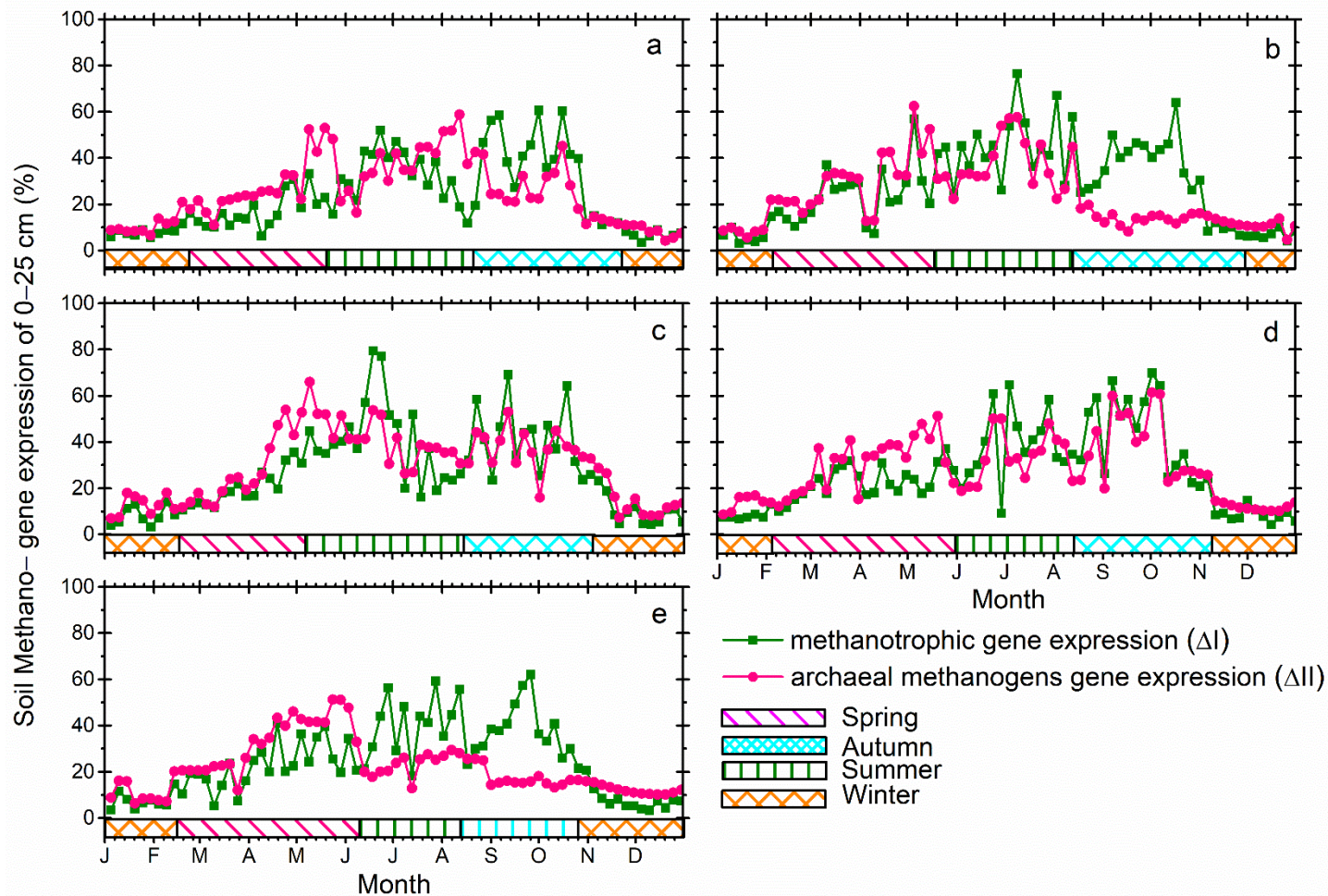


850

851 **Figure 1.** Geographic location of the study site: (a) is a map of China's permafrost distribution, and the red box
 852 marks the approximate location of the Qinghai–Tibet Plateau; (b) shows the study site location and
 853 meteorological stations along the Qinghai–Tibet railway; (c) is the photo showing the study site's
 854 topography and physiognomic. The small red flag in (c) is the eddy covariance tower location; (d) is the close-
 855 up shot of the LI-7700 for methane measurement. *Map boundary and location are approximate. Geographic*
 856 *features and the names do not imply any official endorsement or recognition*

857

858



859
 860 **Figure 2.** Annual patterns of soil methanogen-gene expression of 0 – 25 cm soil depth for years: (a) 2012, (b)
 861 2013, (c) 2014, (d) 2015, and (e) 2016.

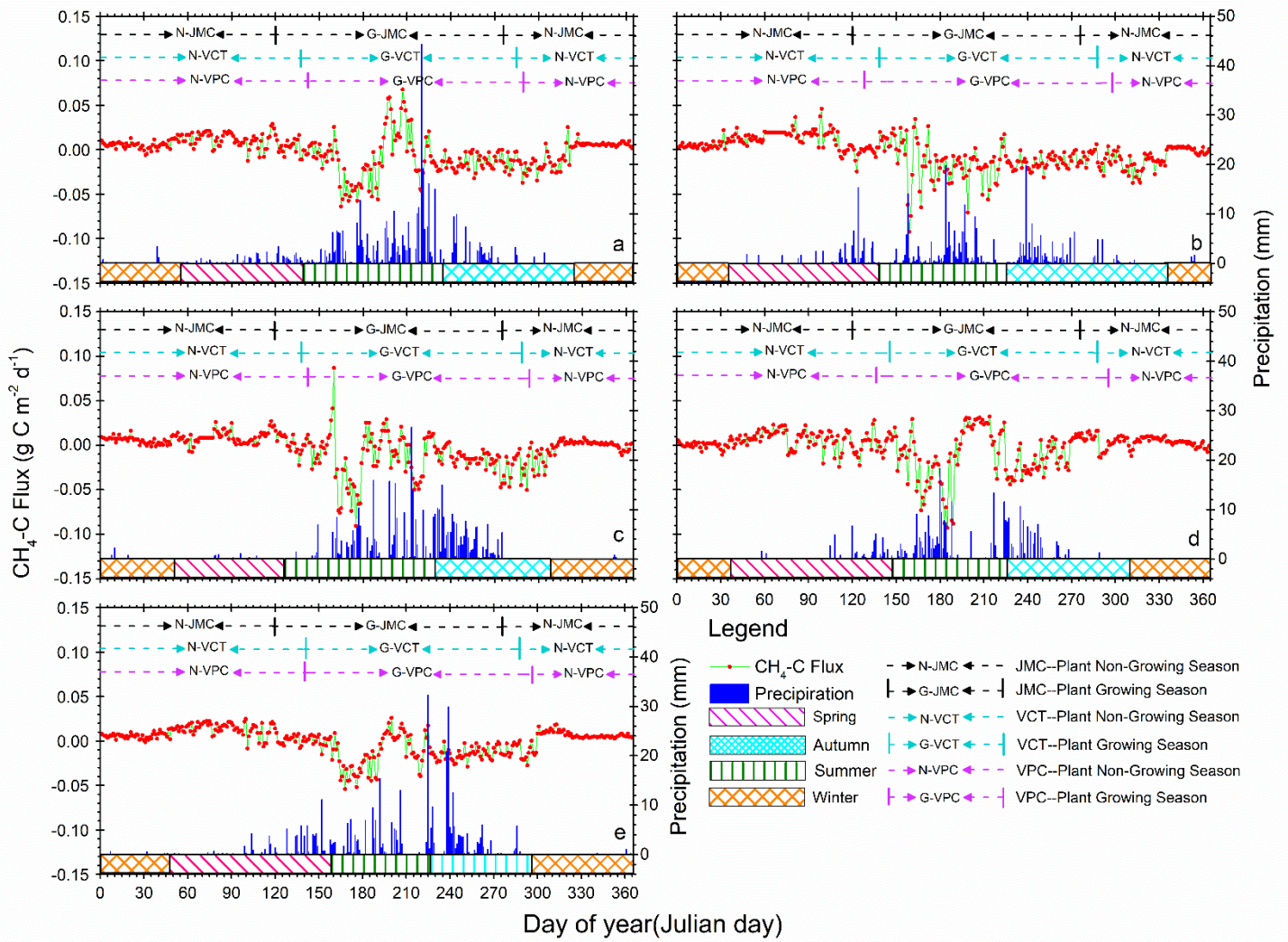
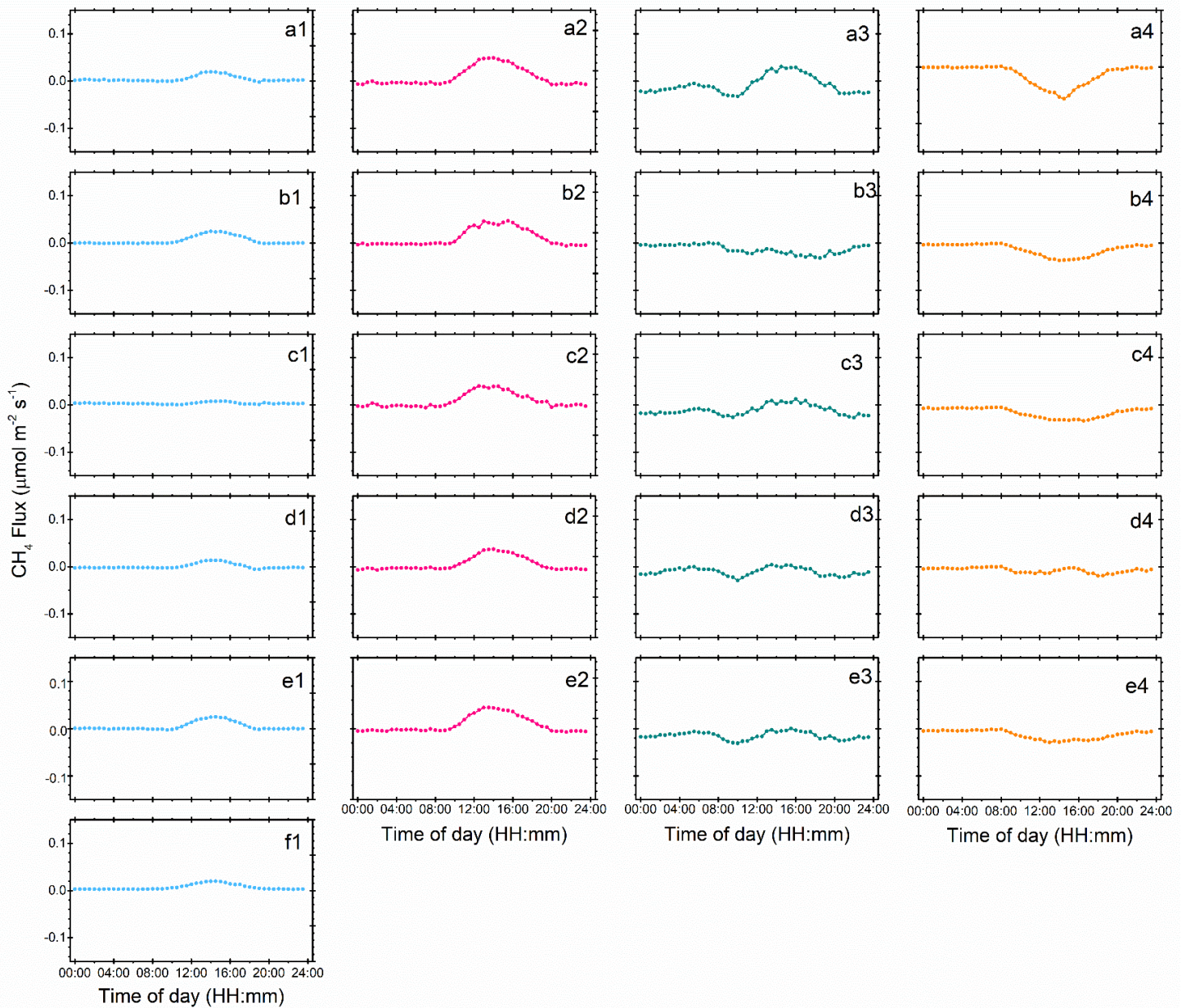


Figure 3. Annual patterns of diel methane (CH_4) flux and precipitation variations from 2012 to 2016. Positive values indicate CH_4 release and negative values indicate CH_4 uptake by ecosystems. Red dots and light green lines are $\text{CH}_4\text{-C}$ flux variation, and the deep blue histograms show diel precipitation accumulation. Pink, olive, cyan, and orange blocks mean spring, summer, autumn, and winter seasons respectively, according to our new method of SMT (see Methods). Black, cyan, and pink dotted lines with bars separated the plant growing from non-growing seasons and stand for seasons by the method JMC, VCT, and VPC, respectively. Details about the methods JMC, VCT, and VPC can be found in section 3.2.



878

879

Figure 4. Diel CH₄ fluxes from 2012 to 2016 for different seasons. Blue, pink, green and orange, represent

880

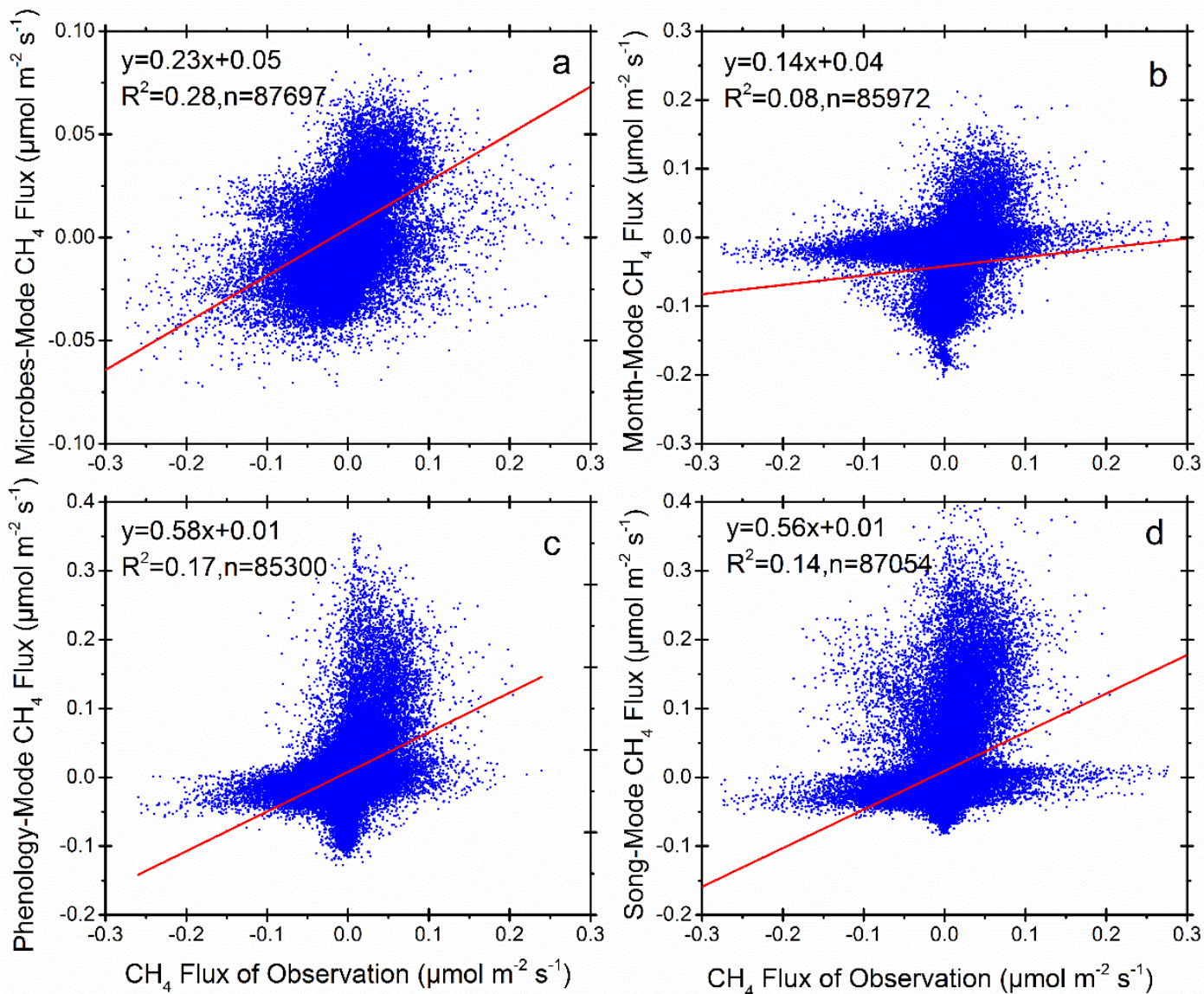
winter, spring, summer, and autumn, respectively; (a1), (a2), (a3), and (a4) are for 2012; (b1), (b2), (b3), and

881

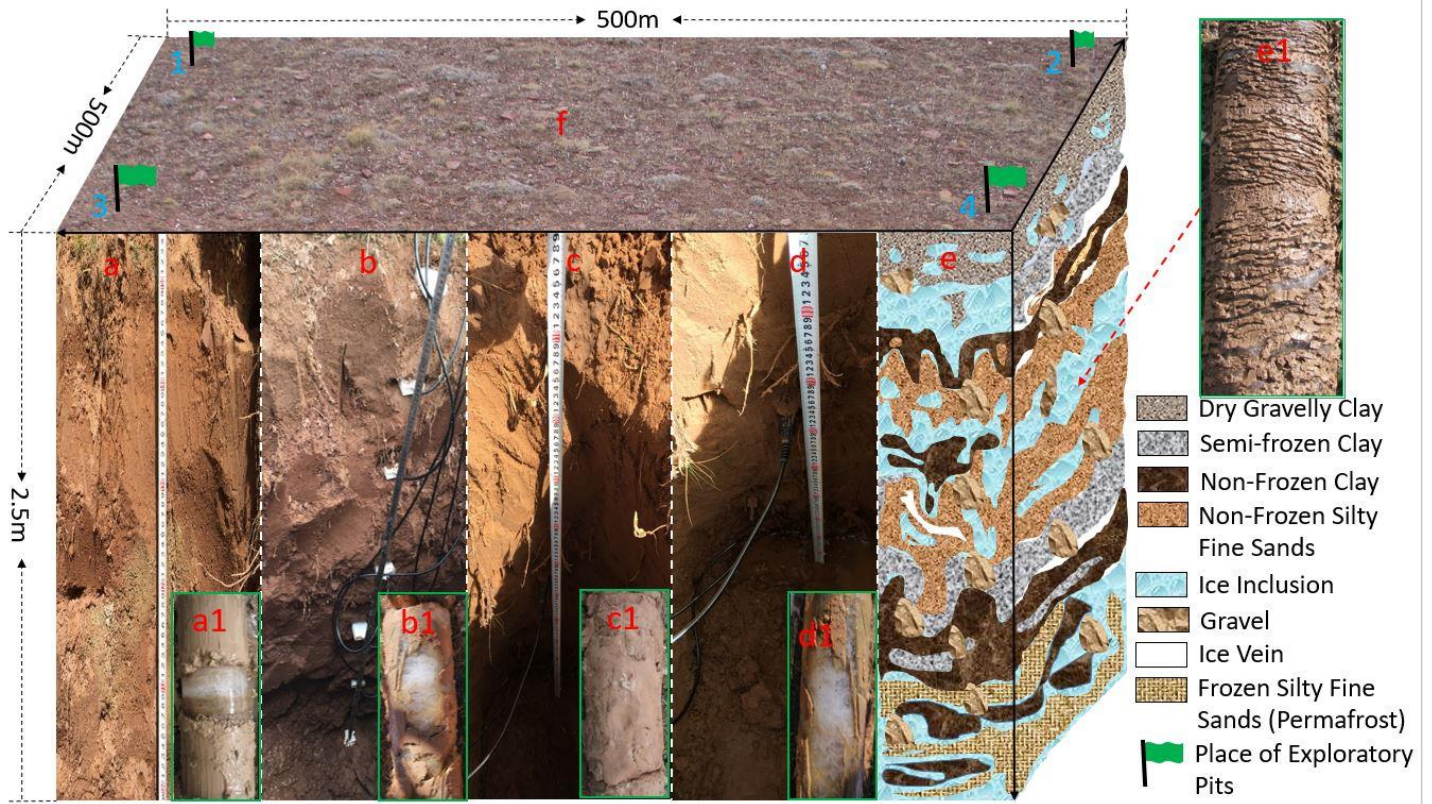
(b4) are for 2013; (c1), (c2), (c3) and (c4) are for 2014; (d1), (d2), (d3), and (d4) are for 2015; (e1), (e2), (e3),

882

(e4) and (f1) are for 2016.



883
 884 **Figure 5.** Regression comparison between observation and modeled methane fluxes with four different seasonal
 885 definitions and classification models. Panels (a), (b), (c), and (d) are for the SMT, JMC, VCT, and VPC
 886 methods, respectively.



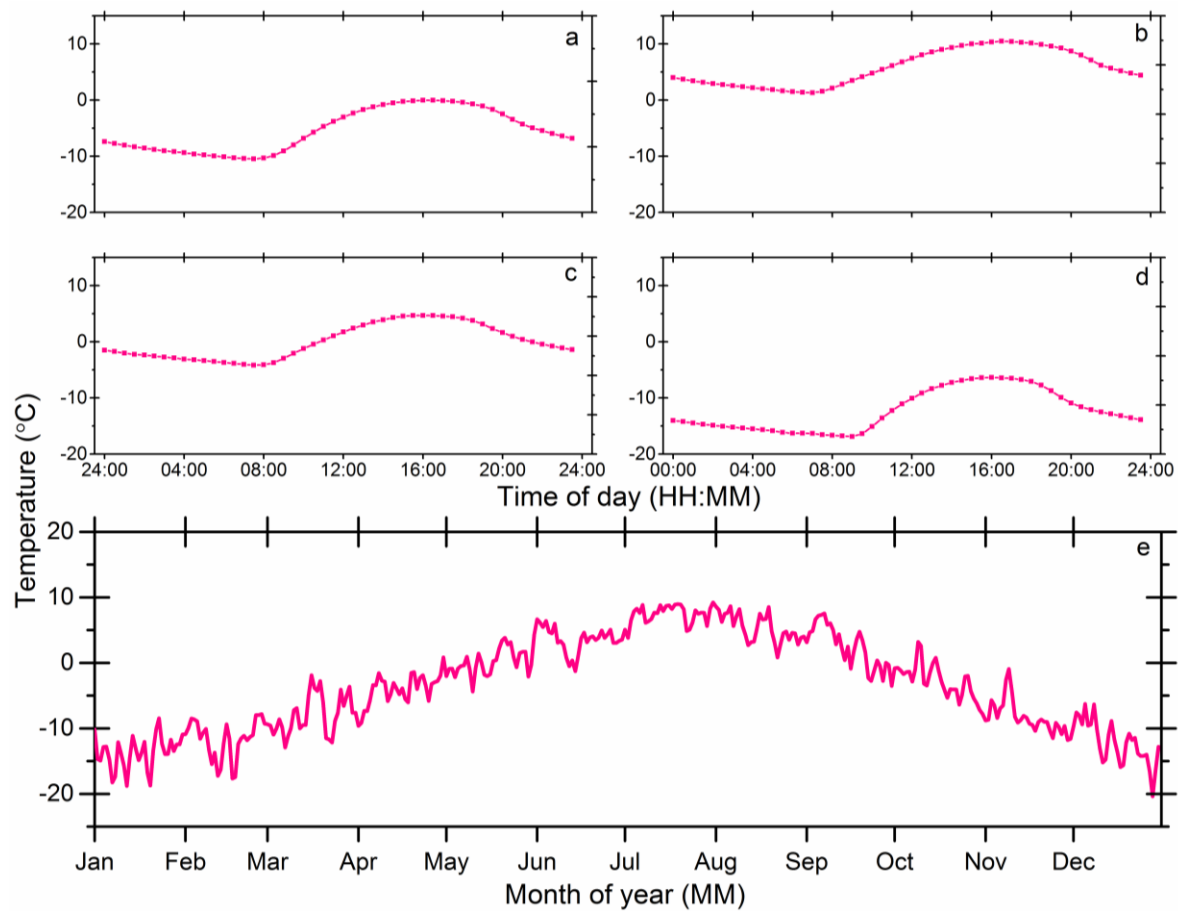
891
 892 **Figure 6.** Location of exploratory pits and drillings in this study in autumn: (f) is photo of a typical ground
 893 surface (October 16th, 2014). Green flags represent the location for the soil survey by test pits and drilling. (a),
 894 (b), (c), and (d) show soil profiles of 0 – 250 cm depths at the North (1), South (2), East (3), and West (4)
 895 corners of the eddy covariance footprint, respectively. (a1), (b1), (c1), and (d1) are drilling cores, with clear ice
 896 (white) in (a1), (b1), and (d1), but not in (c1); (e) provides an illustration that combines results from drillings,
 897 test pits and multi-channel ground-penetrating radar (Malå Geoscience, Sweden) for active layer variations in
 898 permafrost area during the autumn season; and (e1) is a core sample of the same drilling (October 16th, 2014).

904 **Supplement**

905 **Supplementary Table 1** Seasonal soil water content (SWC, %) of winter, spring, summer, and autumn from 2012
 906 to 2016.

Seasonal	Period	10 cm	20 cm	40 cm	80cm	160cm
		Soil Water Content (SWC), %				
Winter	2012 early	0.11	0.08	0.07	0.11	0.14
	2012-2013	0.10	0.08	0.07	0.11	0.16
	2013-2014	0.10	0.08	0.07	0.11	0.13
	2014-2015	0.10	0.08	0.07	0.11	0.17
	2015-2016	0.10	0.08	0.07	0.11	0.16
	2016 later	0.10	0.08	0.07	0.12	0.19
	Average	0.10	0.08	0.07	0.11	0.16
Spring	2012	0.13	0.09	0.08	0.11	0.13
	2013	0.12	0.09	0.08	0.11	0.13
	2014	0.12	0.08	0.07	0.11	0.13
	2015	0.13	0.09	0.08	0.11	0.14
	2016	0.12	0.09	0.08	0.13	0.15
	Average	0.12	0.08	0.08	0.11	0.14
	Summer	2012	0.18	0.11	0.10	0.17
2013		0.16	0.11	0.11	0.19	0.25
2014		0.16	0.10	0.10	0.16	0.24
2015		0.16	0.10	0.10	0.19	0.28
2016		0.16	0.10	0.09	0.18	0.28
Average		0.17	0.10	0.10	0.18	0.26
Autumn		2012	0.14	0.09	0.08	0.14
	2013	0.14	0.09	0.09	0.15	0.20
	2014	0.16	0.10	0.10	0.16	0.22
	2015	0.15	0.10	0.09	0.15	0.21
	2016	0.16	0.10	0.09	0.16	0.21
	Average	0.15	0.10	0.09	0.15	0.21

907

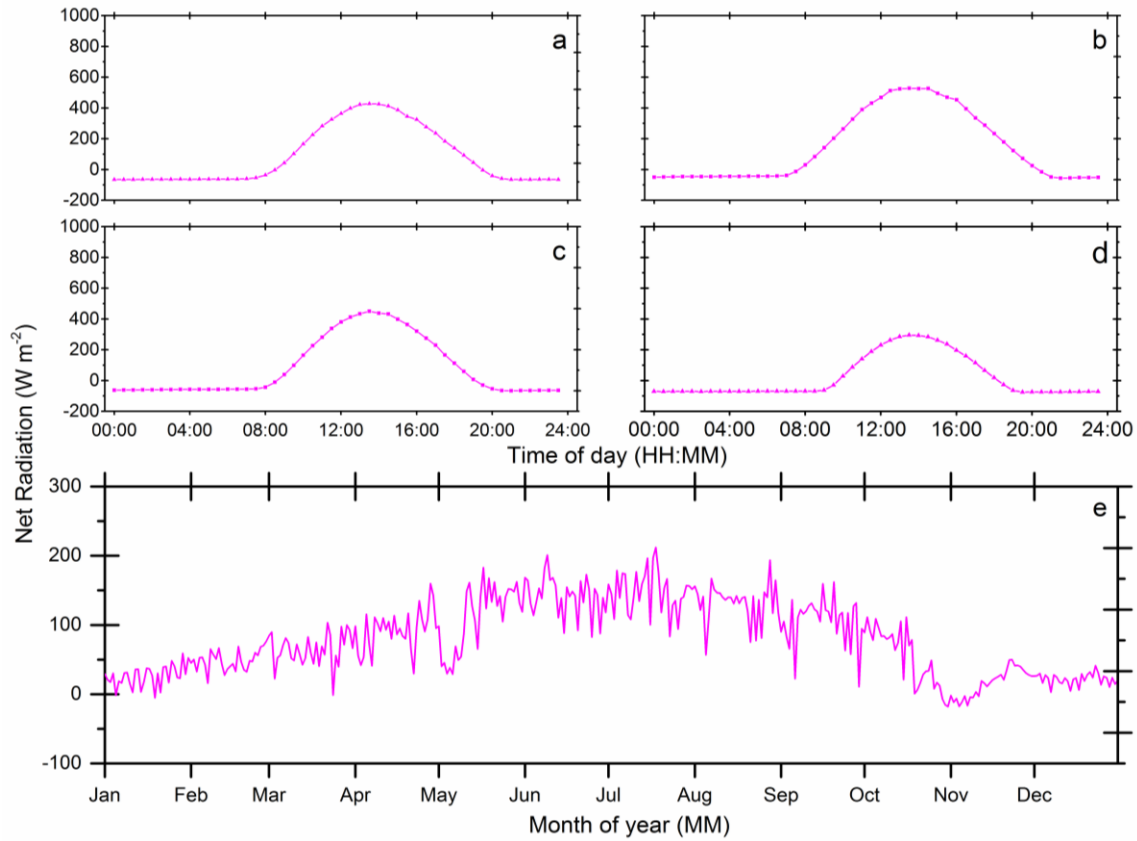


909

910 **Supplementary Figure 1.** Air temperature (T_{air}) measured 3 meters above the ground surface:

911 (a), (b), (c), and (d) are half-hourly mean values in spring, summer, autumn, and winter,

912 respectively; (e) shows diel-scale mean values from 2012 to 2016.



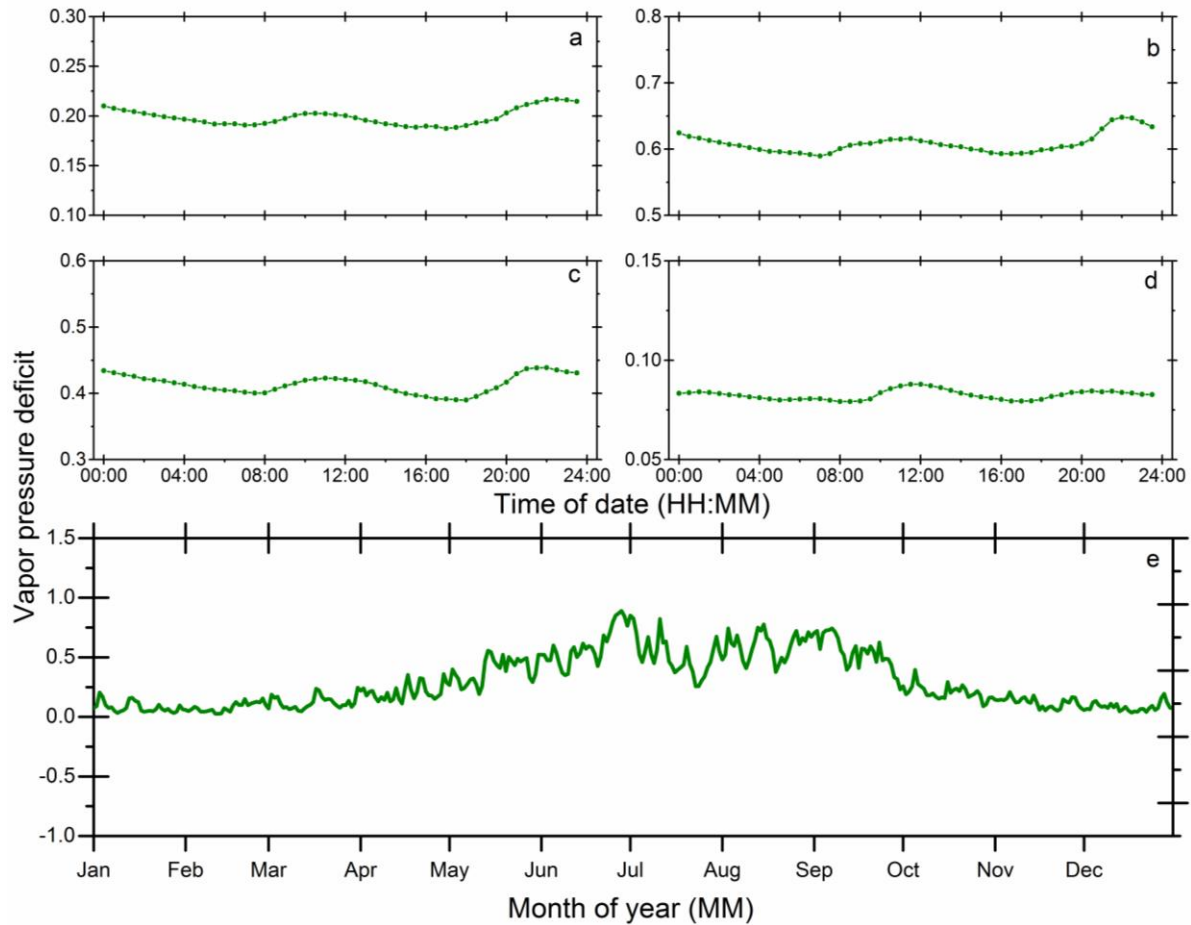
913

914 **Supplementary Figure 2.** Net radiation (R_n) measured 3 meters above the ground surface: (a),

915 (b), (c), and (d) are half-hourly mean values in spring, summer, autumn, and winter,

916 respectively; (e) shows diel-scale mean values from 2012 to 2016.

917



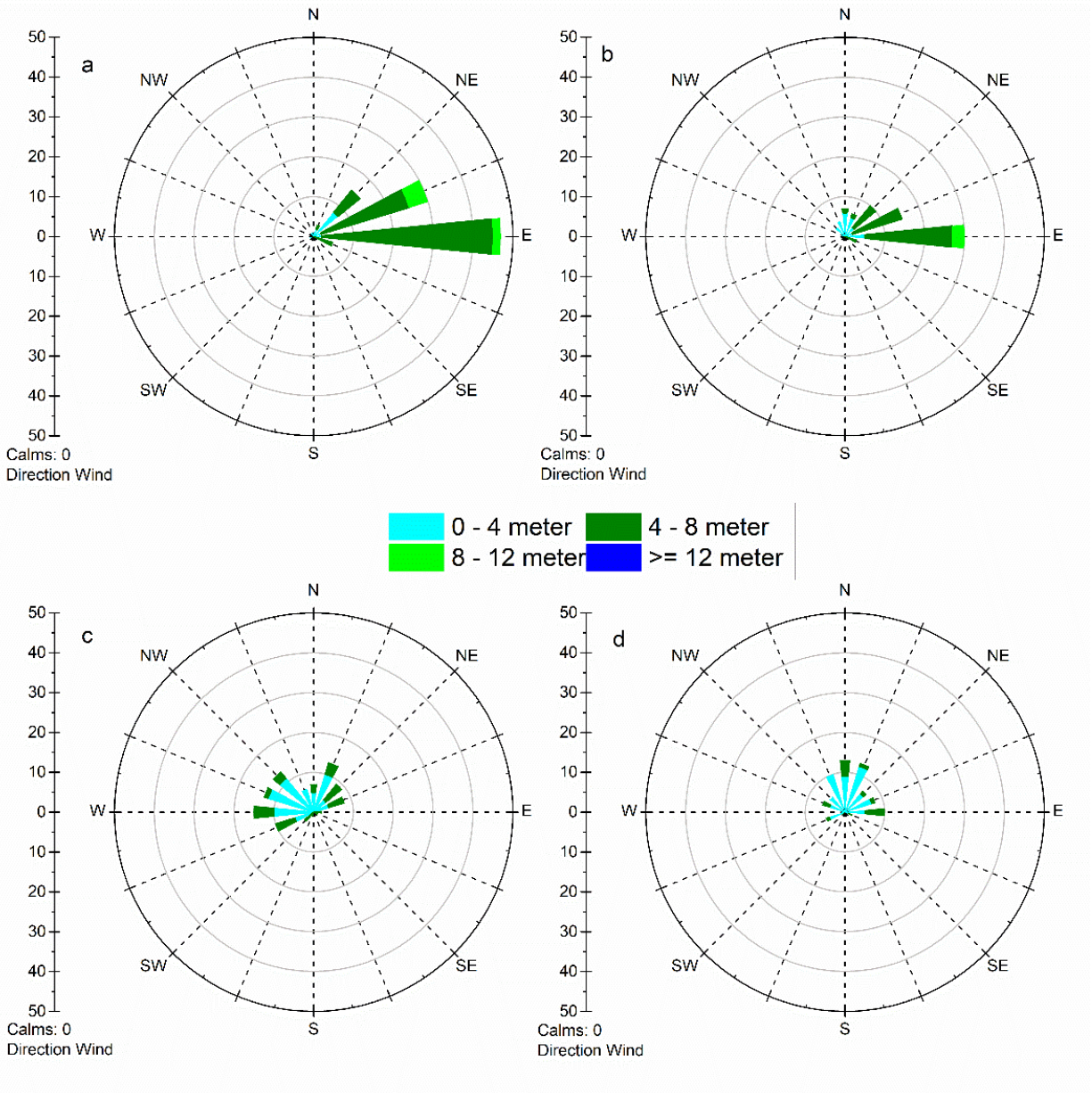
918

919 **Supplementary Figure 3.** Vapor pressure deficit (VPD) measured 3 meters above the ground
 920 surface: (a), (b), (c), and (d) are half-hourly mean values in spring, summer, autumn, and winter,
 921 respectively; (e) shows diel mean values from 2012 to 2016.

922

923

924



925

926 **Supplementary Figure 4.** Diel mean of wind speed and direction between 2012 and 2016: (a) is

927 winter, (b) is spring, (c) is summer, and (d) is autumn. Note the direction of wind means the

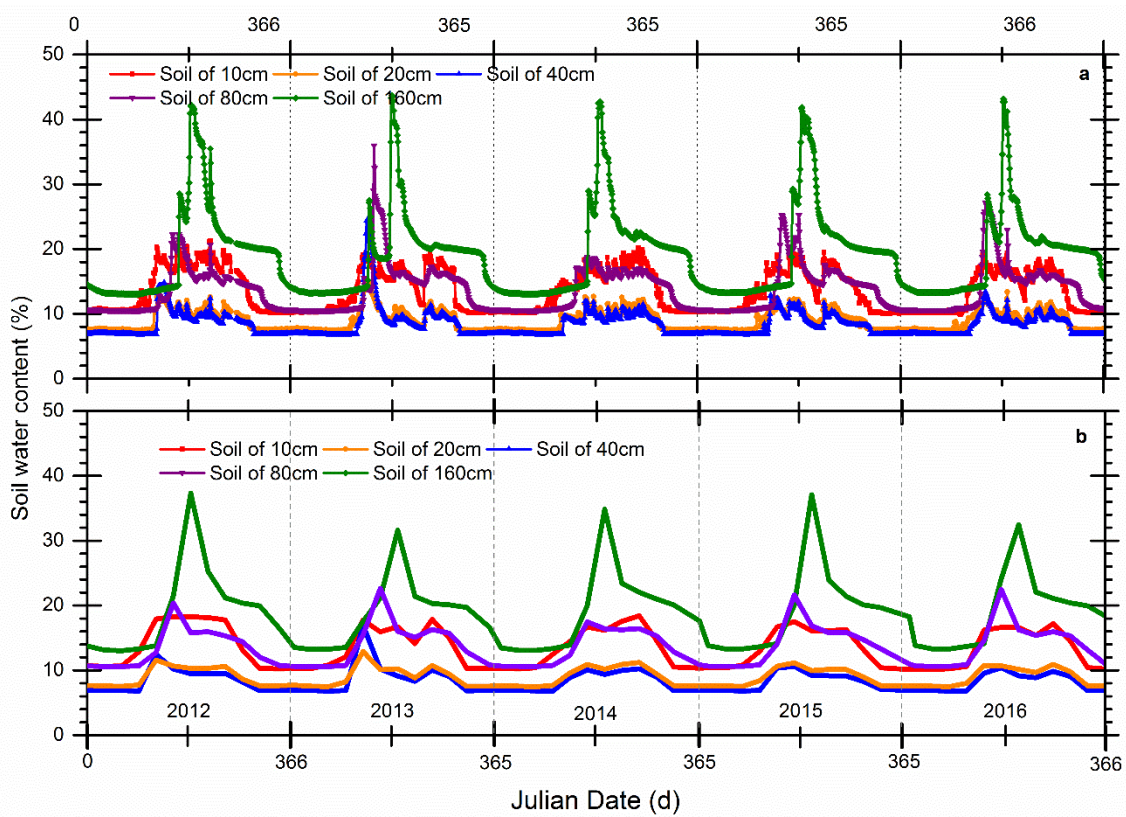
928 direction wind blows *from*. All data are presented as mean values with standard deviations (mean

929 \pm standard deviation).

930

931

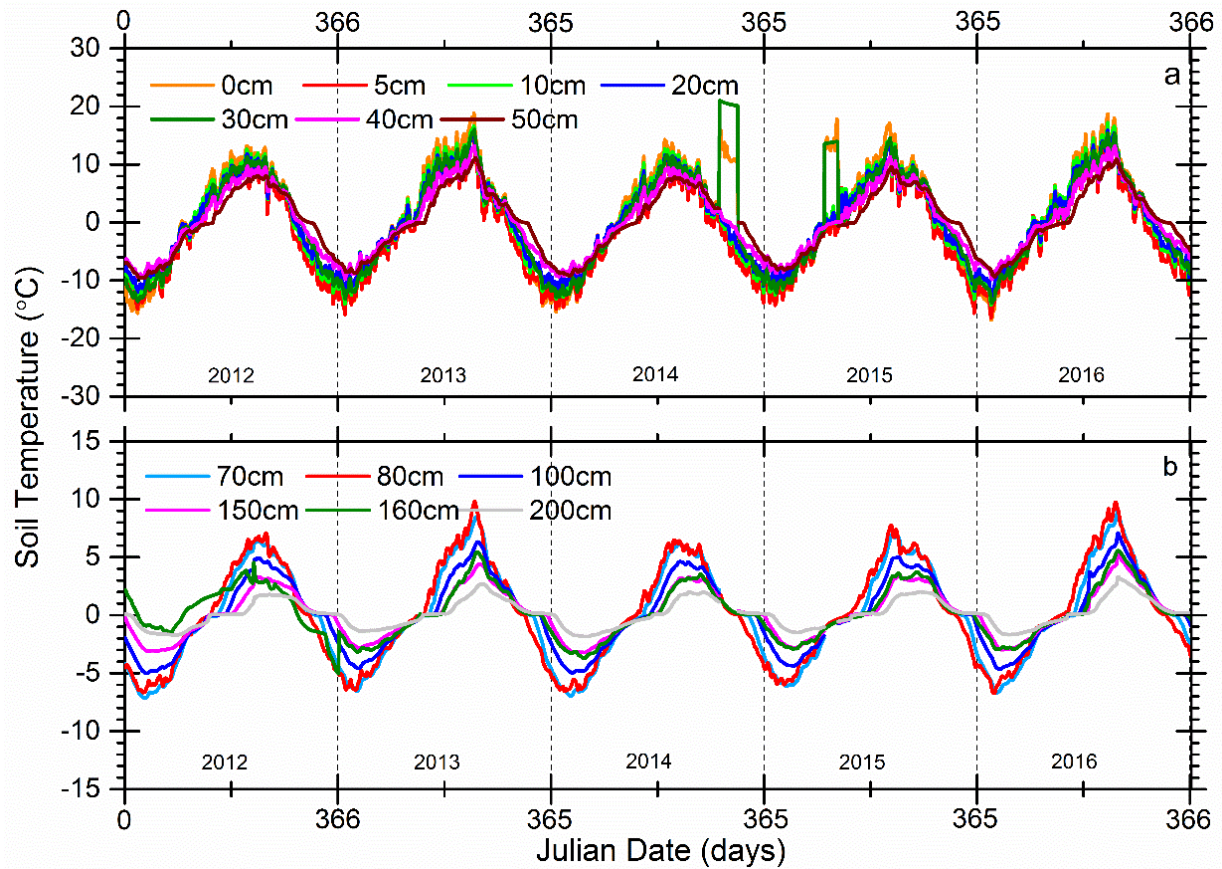
932



933

934 **Supplementary Figure 5.** Comparison between soil water content (SWC) of two different time
935 resolutions from 2012 to 2016, (a) is the half-hourly SWC at soil depths of 10 cm, 20 cm, 40 cm,
936 80 cm, and 160 cm; and (b) is the 4-hourly mean SWC for the same depths.

937

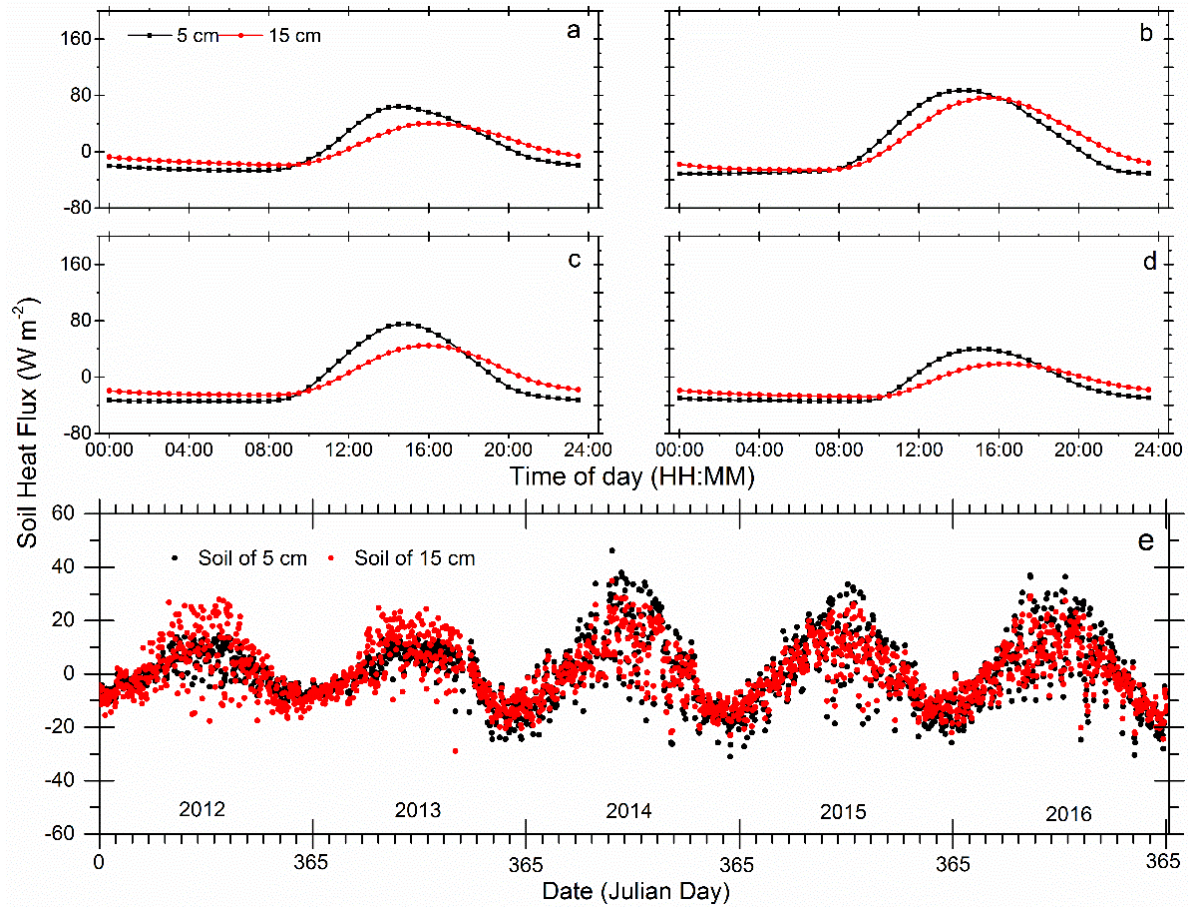


938

939 **Supplementary Figure 6.** Half-hour measurements of 0 – 200 cm soil temperature (T_{soil})

940 variations from 2012 to 2016, (a) is for soil depths of 0 cm, 5 cm, 10 cm, 20 cm, 30 cm, 40 cm,

941 50 cm, (b) is for soil depth of 70 cm, 80 cm, 100 cm, 150 cm, 160 cm, and 200 cm.



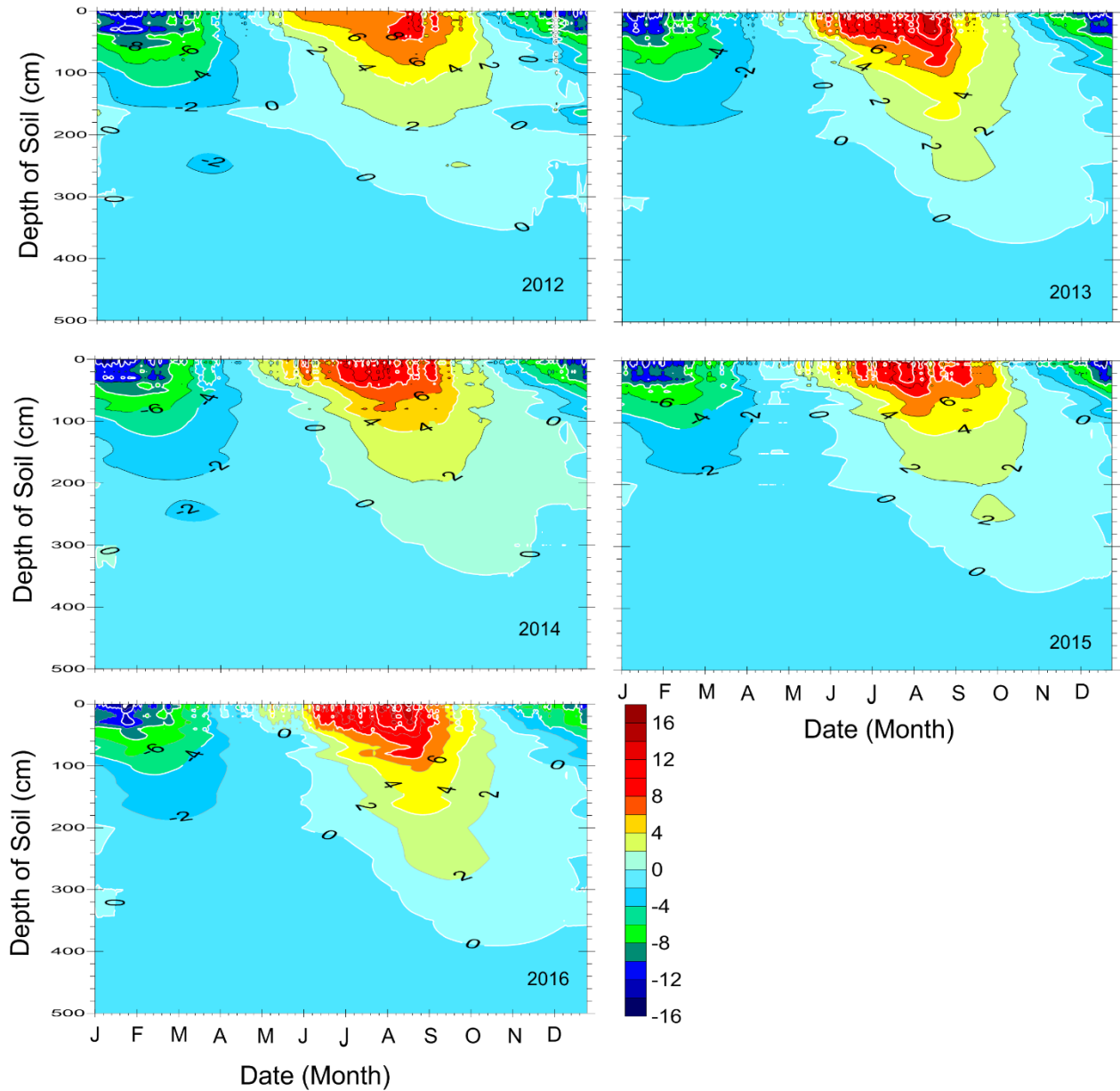
942

943 **Supplementary Figure 7.** Soil heat flux (SHF) at depth of 5 cm and 15 cm: (a), (b), (c), and (d)

944 are half-hourly mean values in spring, summer, autumn, and winter, respectively; (e) shows diel

945 mean values from 2012 to 2016.

946 .



947

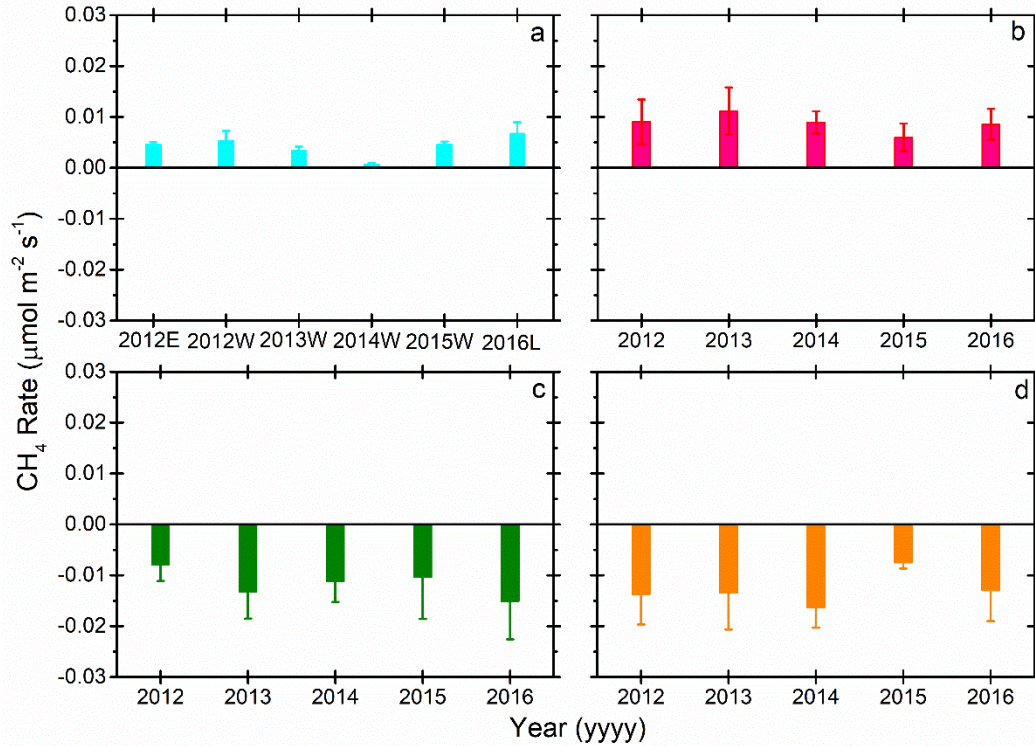
948 **Supplementary Figure 8.** Characteristics of the seasonal freezing and thawing processes of the

949 active layer for years: 2012, 2013, 2014, 2015, and 2016. Different colors represent the soil

950 temperature gradients from -16 °C to 20 °C. The depth of 0 °C represent the active layer

951 thickness (ALT).

952



953

954 **Supplementary Figure 9.** Seasonal CH₄ rate mean value from 2012 to 2016: (a) is winter, (b) is

955 spring, (c) is summer, and (d) is autumn. In the (a), 2012E is started from January 1st, 2012 and

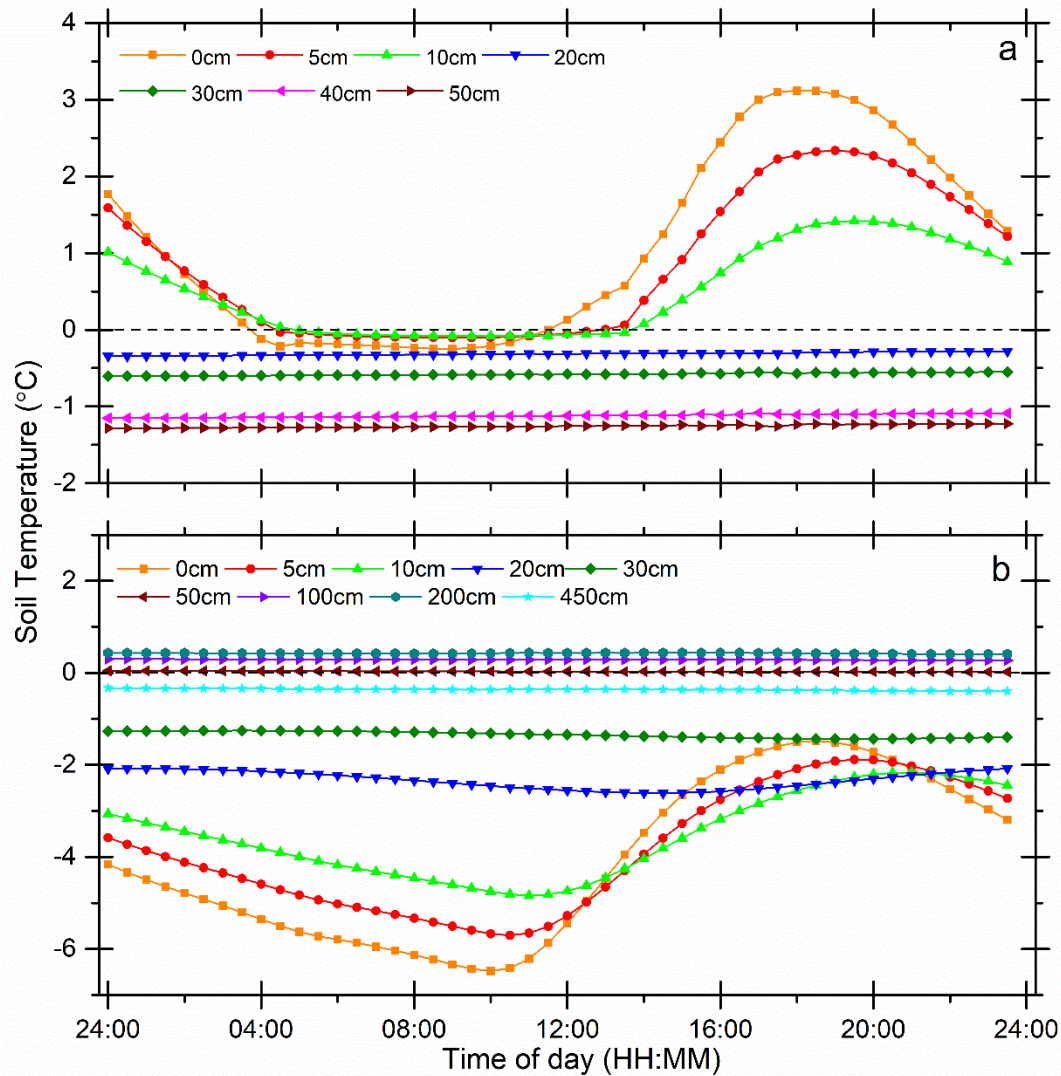
956 ended on February 17th, 2012; 2012W is started from 19th November, 2012 to 4th February, 2013;

957 2013W is started from 1st December, 2013 to 17th February, 2014; 2014W is started from 6th

958 November, 2014 to 4th February, 2015; 2015W is started from 9th November, 2015 to 15th

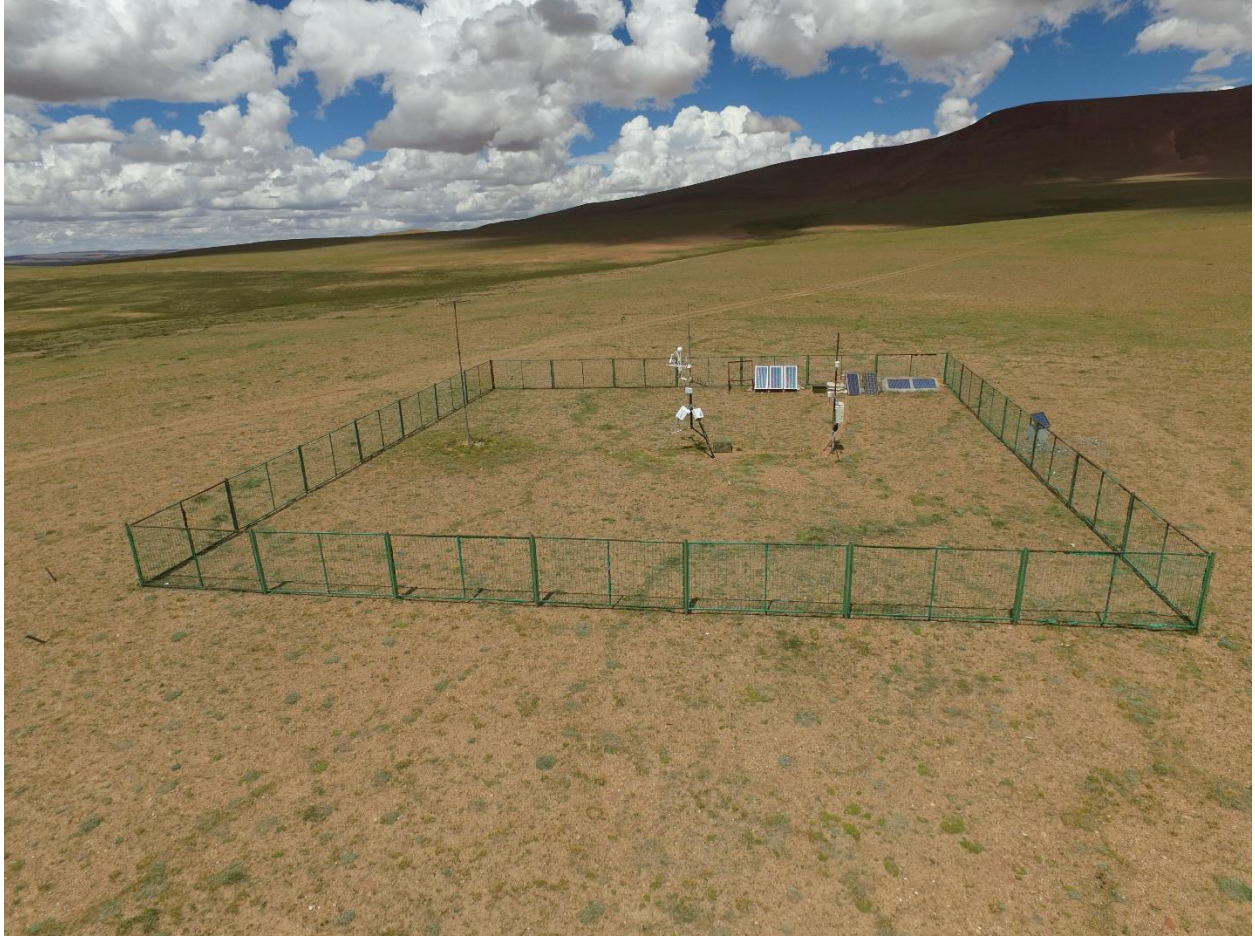
959 February, 2016; 2016L is started from October 26th, 2016 and ended on December 31st, 2016. All

960 data are presented as mean values with standard deviations (mean ± standard deviation).



961

962 **Supplementary Figure 10.** Mean half-hourly values of 0 – 450 cm soil temperature (T_{soil}) from
 963 2012 to 2016, (a) is for spring, (b) is for autumn. Note, that during spring T_{soil} of 100cm, 200cm,
 964 450cm is always below -2 °C and during autumn the T_{soil} of 40cm almost overlap to T_{soil} with
 965 50cm. To make the figure more readable, we removed the T_{soil} values of 100cm, 200cm, 450cm
 966 in figure (a) and removed the T_{soil} values of 40cm for figure (b).



967

968 **Supplementary Figure 11.** A bird's eye view of the eddy covariance site at the Beilu'he station